Proceedings of the 5th NA International Conference on Industrial Engineering and Operations Management
Detroit, Michigan, USA, August 10 - 14, 2020

Reinforcing the internet of things by Neural Network to enhance the Ventilator processes' reliability via Poka-Yoke wirelessly to combat Covid19

Ahmed M. Abed[1, 2]

[1] Department of Industrial Engineering, Zagazig University, Zagazig, Egypt. 44519.
[2] Department of Industrial Engineering, AIET, Alex, Egypt, 21311.
ahmed.abed@aiet.edu.eg, idealstandarddeviation@gmail.com

Tamer S. Gaafar[3]

[3] Department of Computer and systems Engineering, Zagazig University, Zagazig, Egypt, 44519.
Tamer_samy_gaafar@yahoo.com

* Correspondence: Author: ahmed.abed@aiet.edu.eg; (Tel: 01022956165)
Received: 3-7-2020; Accepted: 13-7-2020; Published: 12-8-2020

Abstract

The wireless poka-yoke (WPY) is a novel concept that is concerned with profound control for ventilator processes' behavior to enhance their reliability's mechanisms for its importance after the outbreak of the Covid-19 pandemic. The Ventilator's performance based on rapid controlling some of the influencing variables that reset according to the patient's case. The target is to guarantee smooth traffic O2 flows by controllable the created eddies, which based on impacted variables (e.g., viscosity, Reynolds, and its Circulation value) to create a stationary pressure to push the air to patients' muzzles. The stationary pressure used to create oriented and controllable eddies' paths via controlling the liquid full of ventilator's incubator to maintain the uniform O2 velocity flow. The proposed algorithm based on tackling these variables through (IoT) technology that using sensor data in real-time that can enhance the intervention in-time by Neural-Networks (NN) to predict patient's case changes, and take-over the eddies created to achieve the target. The NN not only forecasting eddies' path and bursting position that makes negative pressure in pleural space of alveoli, to push the air in a regular case. The paper adopts a WPY's perspective that derivative from DMAIC tools to improve processes' reliability.

Keywords

Ventilator mechanism, Reynolds and Circulation number, Neural-Network, Wireless Poka-Yoke, COVID-19.

1. Introduction

In recent years, great interest has emerged in the use of deep learning, especially for tackling problems at the sub-causes level (i.e., unseen mechanism), as the Lean approach recommends (Liu. et al., 2018). The Convolutional Neural Network (CNN) has become well-known among various types of deep controls since its results first appeared in the Image Net Large Scale Visual Recognition Competition (ILSVRC) in 2012 (Krizhevsky, et al., 2012 and Huang.

et al., 2017). The deep-learning emulates data analysis that regarding the sub-causes via remote control of processes' mechanism through IoT, which access to improve the performance and control the mechanical behavior as DMAIC recommended and present the new perception of "WPY" implementation, which is important for providing an interdisciplinary overview for tackling various challenges of any processes' mechanism, such as productivity, environmental impact, reliability and sustainability (Bastiaanssen, et al., 2000 and Gebbers, et al., 2010). Maria Joao Félix et. al., 2019 contribute to find an innovative aspect of simplify, enhance and reliable the processes' mechanism. The result will be processed that have a high-reliability level, which will contribute to lower the slowdowns frequency that puts patients at risk. Society struggle in non-proliferation of epidemics by caring is a respected field, which needs to harness technology to evolve the reliability level that has become a top priority in the improvement agenda of many countries nowadays, especially with the advent of Covid-19. Therefore, medical equipment needs to be smart and have the ability of rapid intervention at-risk cases forecasted. These ideas elevate the design challenges to a new dimension of controlling remotely as named a wireless poka-yoke that alluded by M. Rükmann, et al., 2015 in his future work context. The respiratory device request is in the tops of the countries demands due to the spread of the Covid-19 pandemic. The mechanism of this ventilator based on pumping O_2 gas in steady-state according to five stages for patients' risk cases from A to E. The ventilator must be smart and sensitive to predict influencing variables that help the patients on smooth inhalation and exhalation according to their patients' chest and lung efficiency. This mechanism based on using IoT with respecting Poka-Yoke (i.e., fool-proofing) concept to be wirelessly, and controlled via Neural-Network NN to adapting the ventilator to become suit to the patient according to some influencing variables that measured in time. The proposed mechanism based on processes altering, transmit and direct energy (i.e., compressed air with the specific flow) in a predetermined manner to replace the patient's muscles in performing the breathing work. The profound understanding of this mechanism based on the anatomy of the respiration tract and its main parts (e.g., the lung can be represented as a thin balloon (i.e., alveoli mimicker), has a pleural space, and surrounded by chest wall). If a negative pressure between the chest wall and lung created by the air intake draw, the mechanism will trigger. But the main challenge is continuity of working in a high sensitivity case for predicting to some of the influencing variables affect the patients (e.g., unexplained hyperthermia, the respiratory time (inhalation and exhalation cycle-time) and hypercoagulable) and others on a ventilator liquid incubator (e.g., reservoir) such as liquid's viscosity, the respiratory mechanism time, temperature, muzzle orifice diameter, hose section diameter, Reynolds ***Re***, and its Circulation **Ω** value, which responsible about creating eddies that work to create negative pressure and enhance its outputs.

The lung (mimicked by balloons) has many alveoli full of pressure (Pa) based on twice its surface tension (Ts) divided by alveolar radius (r) according to $P_A = {}^{(2 \times T_s)}/_{r}$. The lung compliance means its working mechanism of inhalation (i.e., expandability is synonymous to high compliance) and exhalation processes of air. The compliance is given generally by volume/pressure and has two aspects (i.e., dynamic and static compliance), the first is based on peak pressure, while the second based on plateau pressure as illustrates in Figure-1. The ventilator must consider these processes in a modular case. The current study focuses on respirator's process improvement, by creating negative pressure in pleural space between artificial lung (i.e., balloons' tides) and chest wall regularly, via moves a fluid eddy

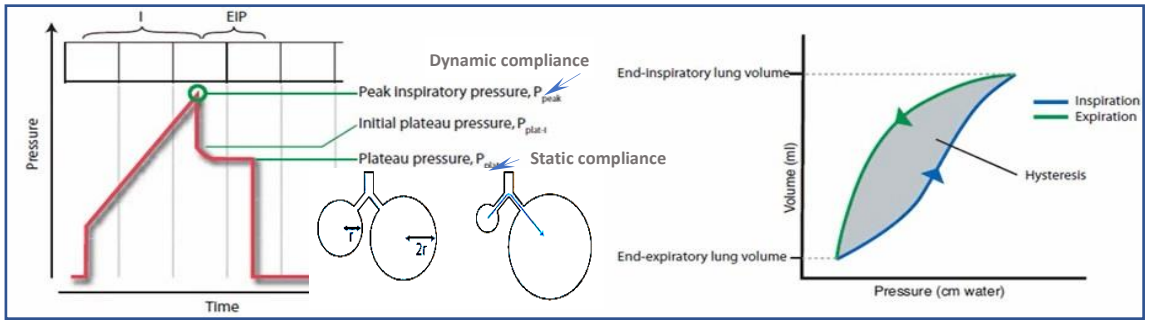

Figure-1: The dynamic and static compliance for inhalation and exhalation

through resistance aisle based on Neural-Network algorithm predominance to press the gas toward the muzzle. This thinking seeking to demonstrate the ability of ventilator in the improvement of its process outputs in a way to suit the patients' case and managing to create a correct balance between the lung muscles and flow stream by distributing these orifice aisles carefully in the face of eddies paths to increase the reliability of process as deduced from G. Ringen, et. al., 2018. The improvement of breathing process reliability as declared by WHO is one of the main means to combat Covid-19, via emerging ICT technologies that relevant for understanding unseen processes mechanism through sensing and forecasting for deviating of influencing variables at upstream. The modern researches recommend using

the Internet of Things (IoT) (Weber RH., et al., 2010) to create patients' medical file using 5G properties to detect a deviation in their biological factors and enable rapid decision making which suits for patient's case (Hashem, et al., 2015) depending on NN capabilities. This concept advocated by Chi M. et. al. 2016, who emphasized the possibility of measurement and the ability to take advantage of big data control in the presence of IoT technology (LeCun Y., 2015 and Kamilaris A., et al., 2017), which offer the abilities to tackle the minor details to revamp a lean concept in deep. The WPY aimed at analyzing the causes and sub-causes forms to improve any process and controlling the breathing mechanisms in the unseen processes affected by one of six causes forms of the fish-bone skeleton. This control considered as a seed of improvement for process reliability as claimed by M. Gregor (2017), via simulation tackling (D.R. Kiran, et al., 2017 and Paloma Diaz-Guti_errez, et al., 2020). This study aimed at imaging and monitoring the “eddy path” occurrences that have the maximum push of airflow, to indicate the sudden disorganization of a slim swirl that occurs when a characteristic ratio of azimuthal to axial velocity components is varied in a common mechanism sector, which is "eddy path" to choose the high compliance alveoli positions in the proposed devise (Abed A., et al., 2014 and Ioffe S., et al., 2015). The axial flow slope designates an internal stagnancy point on the vortex/eddy axis, followed by backward flow in an area of limited axial extent. The burst is a characteristic behavior for eddies when moving through resistance's aisle orifice, which will generate oriented pressure towards the compliance balloon (mimicked to alveolar) that pushes the air toward the muzzle's orifice. Therefore, the researcher must install the material of balloons to face this path to create maximum negative pressure between the balloon and chest wall (i.e., the incubator inner body or reservoir). The core of high vortices discovered at the minimal almost symmetric axis. There is a characteristically, ratable axial component of movement in increment the eddy, or azimuthal component, which must install the balloons to face this direction (Srigrarom S., et al., 2007) and swirling combustors. Similarly, (Aksel, 1992 and Kaya and Jochmann et. al., 2006) numerical computations of the eddy phenomenon collapsing were carried out in a cylinder section of the ventilator's incubator. Under controlled phenomenon circumstances, experiments on vortices confined in hoses were devised by Harvey (Harvey J., et al., 2006 and Abed and Farag 2014), and many others. Most investigators used a cylindrical orifice divergent section as a test section to study the different class of eddy burst to create negative pressure phenomena to full the lung all the pleural space. Moreover, despite empirical, numeral, and theoretical research, eddies become useful if determine carefully its path, which builds on its frame, leftover debatable, and commonly rejected caption has stood out. The goal of the setting realization is to research the reliance on the core eddy disruption class to install the faced balloons on its path. The resultant eddies according to some of the influencing factors such as (feed rate, viscosity, balloon's tissue thickness, muzzle diameter orifice, liquid temperature, respiratory cycle-time, Reynolds number (Re) and circulation number (Ω)) to benefit from created pressure toward fixed muzzle diameter Ø 0.6", as well as for an anti-clockwise flow direction, which visualized when used dye injection.

The fluid mechanism movement is subject to randomly disturbances push researchers to evolve their monitored from the 2D, which based on monocular vision, to a 3D control via a binocular stereovision (P.J. Sousa, et al., 2017). This work based in control on two cameras GS3-U-123s6m offer 4096x3000 pixels resolution at a maximum speed of 28 frames per second to achieve 3.45 μm resolutions per pixel. 3D monitored requires identify the intersection of two optical rays formulated in gradual coordinate system, which calibrated with a special target that undergoes arbitrary motions for resultin eddies [30]. This work aims at controlling deployed eddies via monitored and chases them to burst it, to create negative pressure to trigger the inhalation and exhalation process of the lung, through evolve the sensors of proposed ventilator to control on some of significant factors, which maintain the match stationary for patient's case (C. Bermudo, et al., 2019).

The vital functions of the patient are multiple and it is important to control keeping them at safe limits and levels. Therefore, an accurate prediction becomes easily in the existence of the Internet of Things (IoT) technologies that using sensor data in real-time. Deep Learning (DL) algorithms useful in predicting the equipment function reliability. Srikanth Namuduri et al., 2019 review the DL algorithms used for predictive maintenance and presents a case study of engine failure prediction. This paper discusses the current use of sensors that aided with neural networks in the industry and future opportunities for electro-mixture sensors in predictive performance for a specific process and presents a case study in an international consultant office of ventilators tests.

2. Main Objective

The paper aims to increase the ventilator performance up to 95% - 99%, via reducing the losses paths of eddies created in the liquid, when its trip through resistance aisle to pushing the air toward the muzzle. The proposed problem's tackling illustrates in Figure-2 clarifies the sequential stages through a DMIAC roadmap to control the movement of eddies phenomena via imaging (A.G.Arteaga, et al., 2019) that aided with WPY intervenes as illustrates in Figure 2.(b) flowchart.

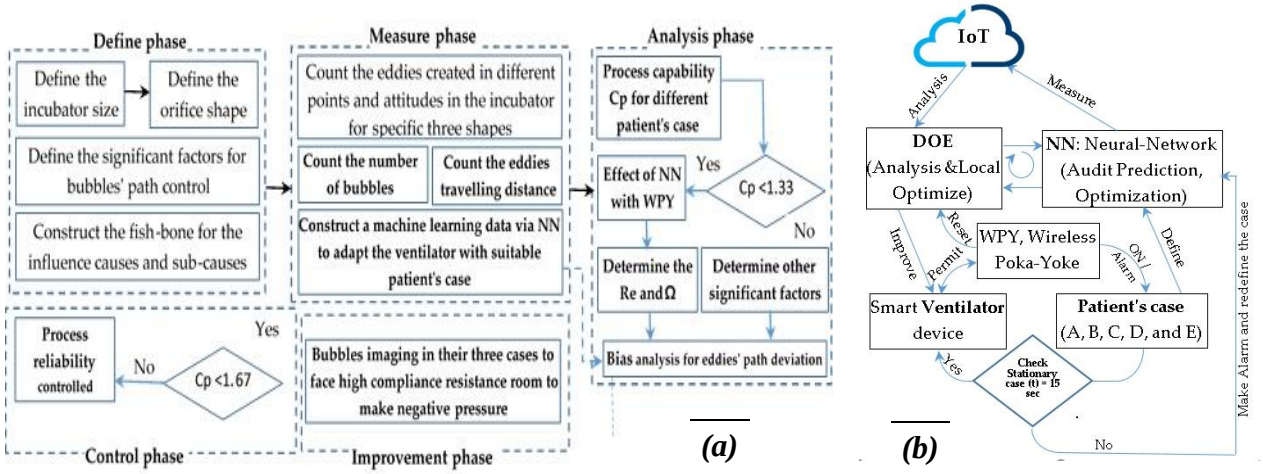

Figure-2 ***(a)*****:** The problem tackling via DMAIC Phases. ***(b)***: The IoT relation with WPY controlling tool.

3. The Define Phase (DOE's Setup and Test Procedures)

A.G. Arteaga (2019) advocates that performance improvement customization is sought based on the control of process's mechanism (M. Fadzly, et al., 2017). Which makes the resource utilization, rate, and cost based on performance indicators that subject to the design of experiments and control. (A.G. Arteaga 2019) also gave us using conditions of a push/pull system (i.e., Kanban) that used to control eddies distributed overall the liquid due to its circulation and affect the reliability. Therefore, the researcher creates a central room in the injection system that controls eddies' paths to trigger the breathing process as illustrated later in Figure-9.

The objectives of this experimental work are to study the effects of interaction between significant factors relating to the mixture proposed liquid used in pushing air via eddies created that cause eddies, and to study their direction of movement (e.g., downstream) during mobility in the hoses. Figure-3, illustrates the "cause and effect" diagram for ventilator mechanism that suffers breathing disturbance due to eddy deviation effects, which created due to the disturbance of pushing air while it being distributed. This problem causes poor ventilator performance for more than 1840 sec/week, which represents 17 heart attack /week. Eddies created and moved undesirable distances go off path, which must be restricted. Thus, the process controlled as illustrated in Figure-4 and analyzing these significant factors to determine which significant, as illustrated in Figs. 5, 6 and 7, which illustrate the importance of elasticity of balloon membrane (i.e., mimic alveoli), and orifice aisles diameter must suit the eddy type. Therefore, the orifice shapes will distributed according to facing eddies paths with different viscosity.

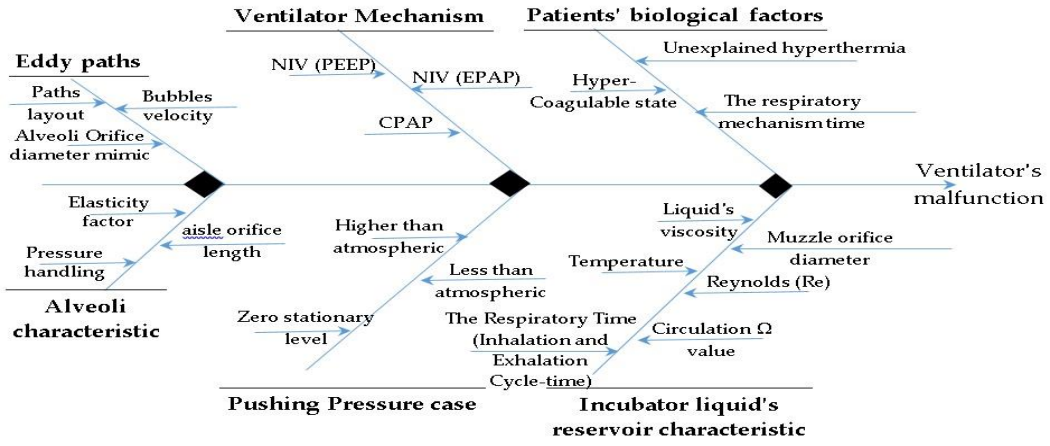

Figure 3. Cause and effect of patient-ventilator process interaction.

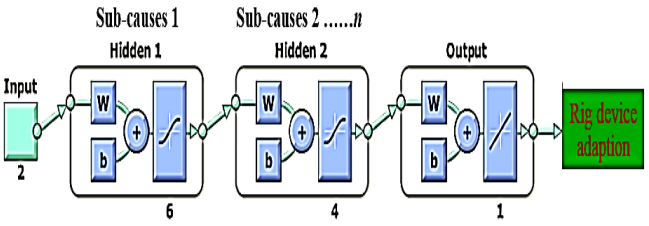

Figure 4: Sub-causes tackling via N-N principals

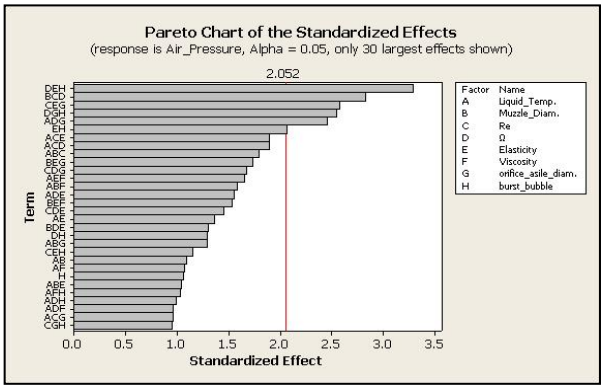

Figure 5: The amount of eddies created of Liquid

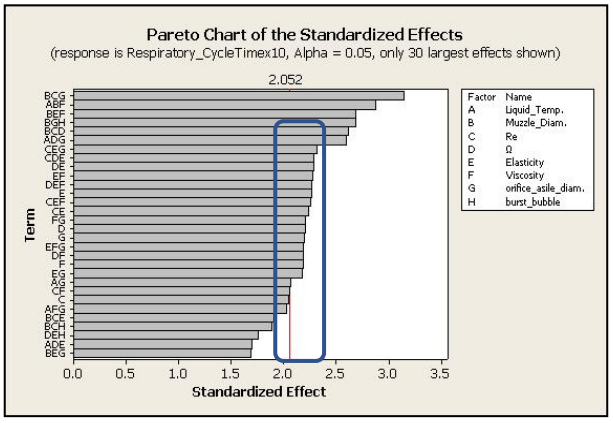

Figure 6: Component sequencing to adjust the pressure

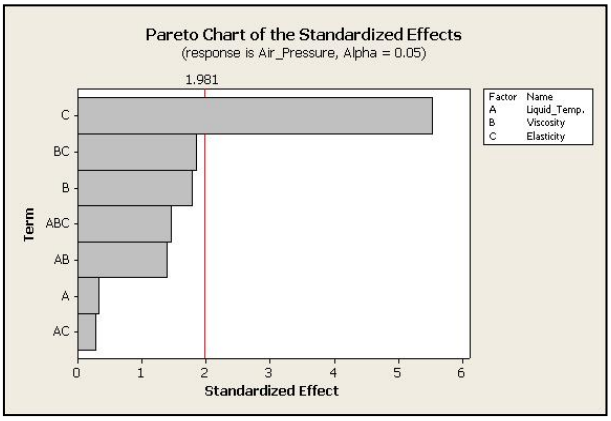

Figure 7: Pressure affected with alveoli elasticity

4. Measurement phase (Ventilator description)

This phase based on eddies path detection preludes to control its path. Therefore, the researcher's interests in classify and identify its pushing effect for air in the central room in a steady-state situation (Lucke, et al., 2019). This work highlights the ability to implement WPY thinking in unseen layers of processes' mechanism with the assistance of imaging techniques to increase its reliability via controlling it through IoT to create central control as K. Chen et al., 2019 recommended, (detecting eddies paths) to get better the robustness of the eddies detection in ventilator processes Xiaofeng, et al., 2020. The work follow to example of (Su J., et al., 2018) when classify the alarm proactive to two levels according to the position threshold (i.e., Level-1: low-severity threshold when bubbles go far away from pleural space orifice and reduce the synthetic negative pressure.) and (Level-2 alarm: high riskiness sill, when all bubbles enter the orifice of alveoli balloon and create tides frequently in pleural space and increase the effect of synthetic negative pressure that accelerates the breath's process). Relevant influence variables are chosen as the minimum-verbosity-Maximum-Relationship standard of level-2 alert to only keep variables with big variance relative to the level of liquid disturbance as discussed by Yuchun Fang et al., 2020. This research highlights to use of flow rate measurement that maintains accurate and stable output value to control eddies' creation and its paths. In some ventilator types that based on single-code pumps, the significant stream rate turns to happen due to rotor-stator interaction. Therefore, the research advocates building smart ventilator control the fluctuations via controlling some of the significant factors (L. Matteo, et al., 2019). In order to test the effect of the key factors illustrated in Figure-3 on eddy creation, the researchers designed and constructed a special prototype test ventilator follows fluid mechanics laboratory with a consultant U.S.C.C house in the 10th of Ramadan city (Egypt). The measurement stage depends on the observed and collected factors,

which were manipulated via the prototype ventilator shown in Figure-8 (i.e., incubation sector) and Figure-9, which illustrates a schematic prototype ventilator diagram (front view) and its Ventilators size description beside the figure. The prototype cistern head distributes its mixture liquid beside the incubator to tackle eddies' movement through two coaxial triangular sections to create negative pressure. The outer cistern designed as a jacket with three sides (23 x 23 x 23 cm) made of transparent acrylic sheet 0.15 cm thick. A part of its base was made of a transparent acrylic has, 18x18 cm, to facilitate the visualization of the vane-setting angle. The inner cistern is also made of acrylic sheet with dimensions of 12cm x 12cm x 23cm and fixed coaxially with the inner cistern diameter.

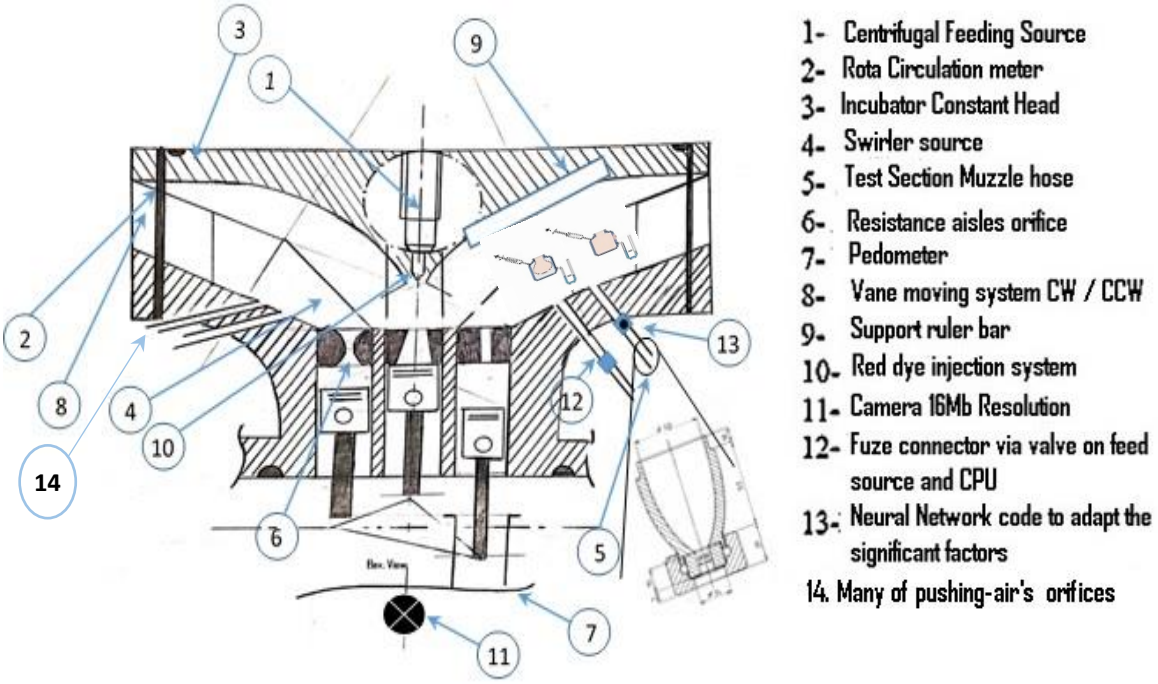

Figure 8: The prototype of the incubator's liquid sector layout.

This ventilator designed to measure the result of changes in the interaction of significant factors illustrated in Figs. 5, 6 and 7. The three sides of the inner incubator's jacket (i.e., chest wall of incubation) cistern have 132 holes have special positions faced eddy paths as illustrated in Figure-9 later, which illustrates three stages or rooms (A,B and C) of this mechanism. The liquid creates eddies that move through holes to create negative pressure via tides actions to triggers the lung work, these holes distributed from 0.03 cm to 0.1 cm diameter according to eddy type. The central room orifice represents the resistance between high compliance alveoli and low compliance airways, and located 10 cm below opening of the muzzle's orifice. The swirled entrance tackled by two-orifice direction, with length 4mm (cylindrical section) & 15 mm (Cone section) were used to determine effect on the eddy phenomena. The two orifice have constant inner diameter of 1.5 mm. The vanes were fixed axially at a radius of 1.0 cm. The amount of swirls transported on the fluid influenced by the vane angle tuning, Φ, and the feed rate. It was necessary to design a precise pictorial WPY experiment to study the movement of eddies (created from eddies) and sequential changes for the vane angles, as a prelude to control the travelling distance of eddies and achieving the Lean objective. The resistance room fixed vertically, with the lower plate of the eddy during two verges and equipped with a holder with 15 orifices with a bore diameter ranging from 0.03 to 0.5 mm. Because of altering (Re) numbers from 690 to 7312 (cylindrical section), 885 to 10837 (cone section), the swirl vane angle distribution (i.e., circulation number Ω) was controlled for counter-clockwise flow directions, because they have a direct effect on eddies caused by eddy burst in a zone ahead of the burst (i.e., pressure range effect). A scale pasted on the incubator surface to monitor and measure the location of the eddy created and burst it.

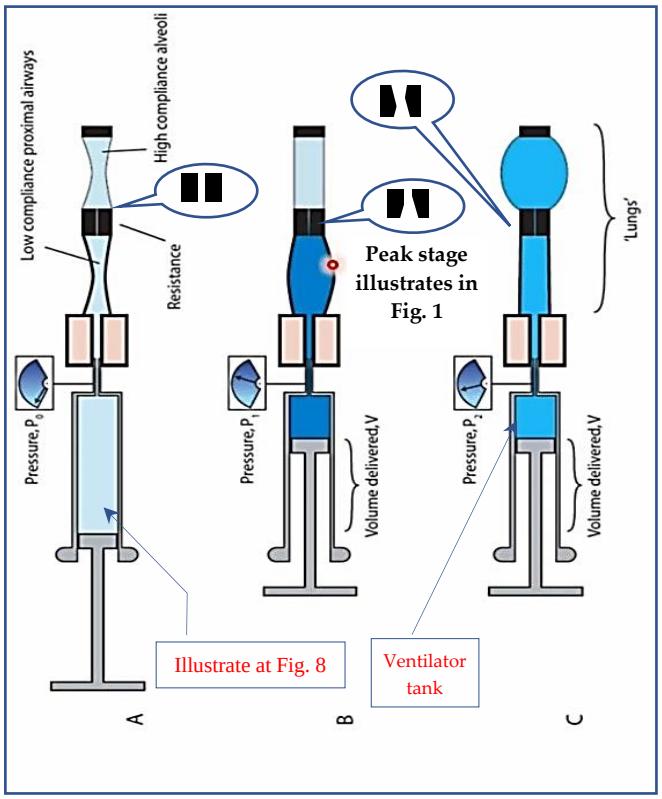

Figure 9: Static and Dynamic compliance at holes

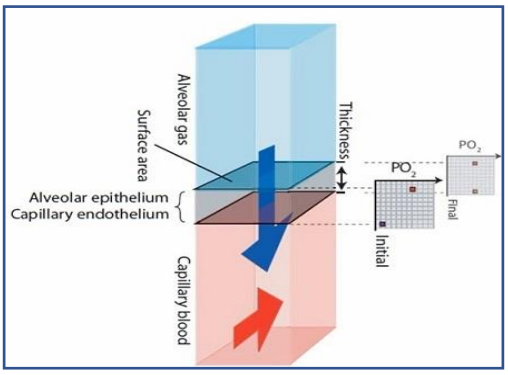

Figure 9.1: gases air exchange among alveoli and capillaries

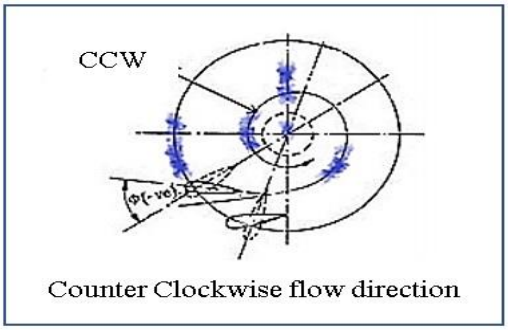

Figure 10: The two vanes angle-setting viewer from top

5. Control Phase

The ventilation mechanism measured for a given class of eddies that are subject to vary from other classes (Russakovsky O. et al., 2015). Two incidents of each type of eddies with various ranges are generated and considered as input **P** of the system. The gas exchanges based on barrier's thickness that treated like a layer of water that work on control of O_2solubility in barrier as illustrated in Figure 9.1. Eddies affect pressure types are:

Eddies class 1 (P1): P is the gradual response to a second order system G(s)=1/(20S^(2+0.5S+1)) with a step of Range 20, and the test occurrence is generated with a step of range 15.

- Eddies class 2 (P2): P is a step of Range 3 for the training occurrence and Range 2 for the test occurrence.
- Normal operation (N0): all samples before the introduction of eddies constitute the normal operation data.

This stage focuses on imaging the position of eddy creation and its evolution until move through resistance aisle (eddies case), and analyzing the sub-causal factors via a Neural-Network (NN) model (Yosinski J., et al., 2014) to suggest the modification process until the eddy push its space and create negative pressure as illustrated in Table-1. These standards tackled via Minitab$^{(v.16)}$ to detect the significance of setting muzzle's orifice diameter. In Eq. 2, describe the NN structure as illustrated in Figure-4, where ***h(t)*** is the diffusion speed output at time ***t*** (at rest 0.75s:0.25s at sea level), which inversely proportional to the cardiac output also to allow gas exchanged as illustrate in Figure 9.1, and depends on the layer thickness between alveoli and capillary that treated as illustrated in Figure 10 and input $x_{(t)}$ for significant factors inferred from Figs 5,6 and 7, also depends on learned pressure **P**. The need to seeking the significant factors (including Max flow, feed-rate, pressure, *(Re)*, viscosity, kinetic viscosity, liquid temperature, respiratory cycle-time, muzzle orifice, and hose sections diameter). The NN that connected with a sensor used to predict the accurate values especially (*Re*) based on Eq. 1 (S. Melzer, et al., 2019) to maintain pushing air in stationary situation also.

Table 1. The effected factors on incubation's liquid ventilator sector at WPY.

Effect Factors	Levels		Effect Factors		
	Low	High		Low	High
1. Liquid Temperature	19 ºC	47.41 ºC	5. Circulation number [Ω]	1.135	1.286
2. Ambient Temperature	5ºC	50.56ºC	5.1. Vane angle Anti-CW	-7.4º	-2º
3. Muzzle diameter	4 mm	9 mm	5.2. Balloon's Elasticity	+2.5	+12
4. Reynolds number (*Re*)	662	3312	6. Kinematic viscosity m^2/s	12	15
4.1. Ø Orifice aisles (A)	8mm	12mm	7. Air Pressure	200 Pascal	300 Pascal
4.2. Ø Orifice aisles (B)	11mm	13mm	8. Respiratory cycle-time	2.5	7 sec
4.3. Ø Orifice aisles (C)	10mm	15mm	9. Viscosity	100	486.67

$$(\boldsymbol{Re}) \quad = \rho * v * {}^{D_H}/_{\mu} = Q * {}^{D_H}/_{vA} = {}^{internal\ \ force}/_{viscocity\ \ force} = \frac{(mass\ \times acceleration)}{dynamic\ \ viscosity\ \times area\ \times \frac{velocity}{distance}} = \frac{\rho * \frac{L}{\tau} * L}{\mu} = \frac{vL}{V} \ldots\ldots (1)$$

$$h_{i(t)}^{m} = \sum_{j=1}^{N_h^{m-1}} (W_{i,j}^{m} . y_j^{m-1} + b_j^{m})_t \ \ldots\ldots\ldots (2) \qquad \text{While,} \qquad y_i^m = A(h_i^m) \ldots \ldots\ldots (3)$$

Where,

$\boldsymbol{D_H}$	Hydraulic incubator diameter	$\boldsymbol{M_A}$	Muzzle's hose cross section area m^2
$\boldsymbol{\rho}$	Density of the fluid kg/m^3	$\boldsymbol{v}$	Kinematic viscosity m^2/s
$\boldsymbol{V}$	Velocity of the liquid bubbles m/s	$\boldsymbol{\mu}$	Alveoli elasticity membrane $N.s/m^2$
$\boldsymbol{L}$	Linear dimension m	**y**	The output prediction for deviation

While In Eq. 3, the function ***A*** represents the activation function. In this section, we examine effect of several eddies types for describing pressure flow. The pressure flow in the ventilator system is in general unsteady. In most regions, it is disturbance due to the systolic or diastolic pumping used to suction of ventilator from intermediate room as cited by S. Melzer et. al., 2019. The Pressure, viscosity and velocity variables vary periodically with time and have direct impact on process efficiency. A dimensionless parameter called the Womersley number,α,Where β the radius of the orifice section is, ω is the frequency of the suction wave in radians/sec, and v is the kinematic viscosity. $\alpha = \beta\sqrt{\frac{\omega}{v}}$ This definition shows that the Womersley number (Weissenbrunner, et al., 2015) is a composite parameter of the Reynolds number $= 2\beta u/v$, and the Strouhal number $S_t = 2\beta\omega/u$. The square of the Womersley number is called the Stokes number. The Womersley number denotes the ratio of unsteady inertial pressure to viscous forces in the orifice sections flow. Cylindrical coordinates *(r, θ, x)* where *x* is the axial coordinate, *r* is the radial distance from the *x*-axis, and θ is the circumferential (azimuthal) angle. The axial flow velocity in a orifice section of radius, u= u(r) = $\frac{r^2-\beta^2}{4\mu}({}^{dp}/_{dx})$, where ${}^{dp}/_{dx}$ is constant pressure gradient, as shown in Figure-9 and equals $\left[{}^{(p1-p2}/_{L}\right]$, where L is the length of the orifice section, which is defined above. Therefore,$u(r) = (\frac{\beta^2\Delta p}{4\mu L})(1-\frac{r^2}{\beta^2})$, The maximum velocity occurs at the center of the orifice section, *r= 0*, and is given by: $u_{max} = (\frac{\Delta p\beta^2}{4\mu L})$, according to J. Steinbock, et. al., 2019, Velocity measurement is used for flow rate controlling in various industries within a fully turbulent flow rate via analytical formulation for the Reynolds number dependence of the profile is derived. The turbulent flow of studied liquid in a orifice section with an inner diameter D= 48 *mm* is considered. The straight cylindrical orifice section downstream of the double elbow has a length of 60D as shown in Figure-11. The volumetric velocity is fixed to be *u* = 4.19 ms^{-1},

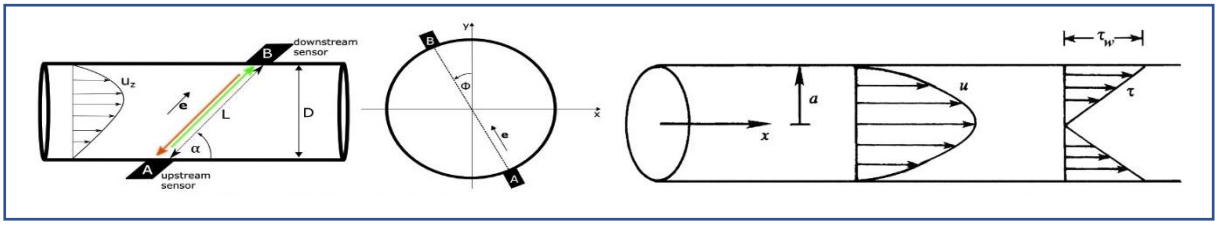

Figure 11: Impact factors for forces into muzzle path.

which corresponds to a Reynolds number of about *Re*=0.310[3]. In order to perform the numerical simulations in this setup was used and resultin appeared in Figure-14. The Reynolds-averaged equations were solved with the closure

model κ-ω from Wilcox, which shows the eddy viscosity models results among in a section flow as suggested by A. Weissenbrunne, et. al., 2016.

5.1. Experimental Results of incubator pressure output

The control revealed that eddies have three creating types: two of these classified as wide spiraled or smooth flattened, while the third called "axis-symmetric". The (Re) and **Ω** have a direct influence on bubble path and eddy creation, and must be set at 1600< (Re) <1800 and 1.15< **Ω** <1.18 as illustrated in Figure-12. The feed-rate increases to 170 with low viscosity 127 mPa with save the other factors as illustrate in right box into figure as illustrated in Figure-13. The vane angle is set anti-clockwise, between {10:12}. The kinetic viscosity is fixed at 55.5 MPa at all factors, and the process interacts with its pressure and robot arm angle, as illustrated in Figure-14, whether the contour illustrated in Figure-15 is set at 1400< (Re) <1800 if the vane angle set at 10^{0}.

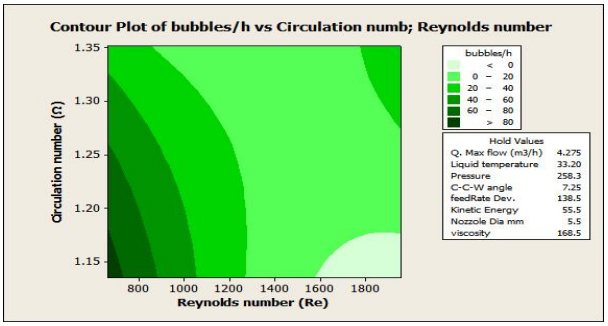

Figure-12: The contour plot of eddies/bubbles/h under Re and Ω

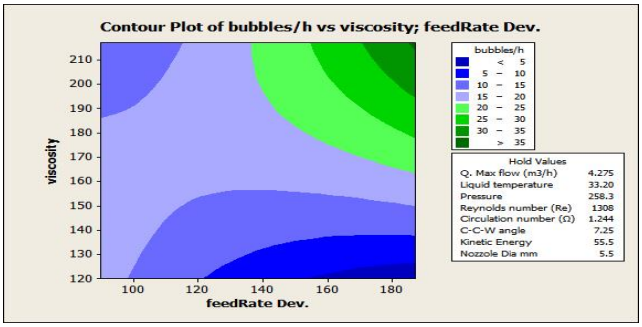

Figure-13: The contour plot of eddies/bubbles/h under feed-rate and viscosity intersection

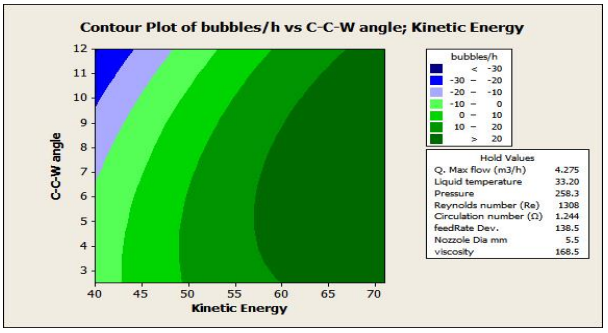

Figure 14: The contour plot of eddy/bubbles/h under kinetic viscosity and anti-clock wise angle direction

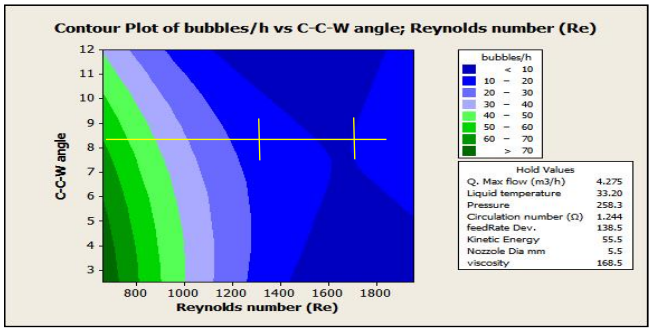

Figure 15: The contour plot of eddy/bubbles/h under ***Re*** and anti-clock wise angle direction

Figure-16 illustrates how the suggested inputs of optimization values start the NN model running to increase the process's reliability, for main factors, to reduce rate of defective ventilator to 5 ppm. Sets of Experiments were

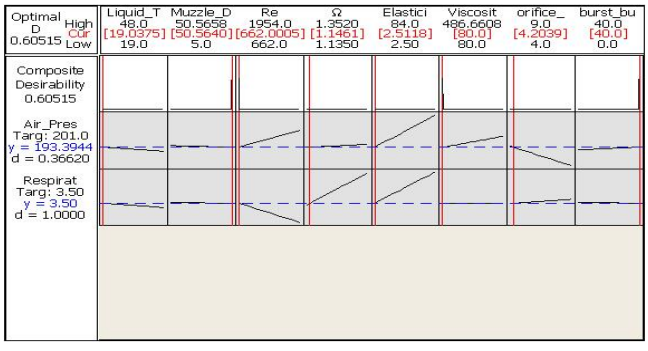

Figure 16: "The optimization values for all significant factors to decrease ventilator's slowdown"

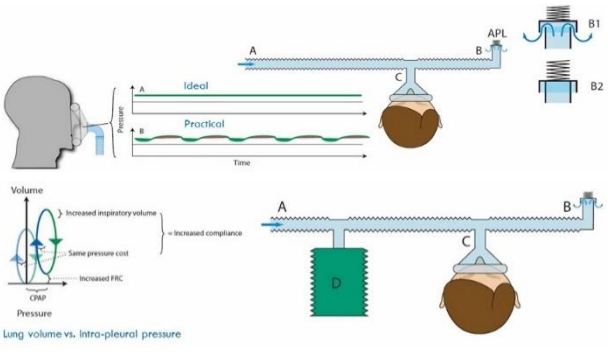

Figure 17: "The muzzle's hose distance between two nearest point"

performed fixing 622< (Re) <1954, while 1.083 <**Ω**<1.38, and the vanes' angle was suggested to be 47°, while the viscosity was 127.63. For each vane's angle and its rotation, the disturbance effect flow was observed and the axial eddies that appeared was recorded

5.1.1. Eddy Burst class types

The types of eddies classified and described via injecting red dye ink into the incubator's fluid, which monitors its movement paths, and classified eddies type, as follows:

5.1.1.1. Type 1 – Wide spiral class eddies

The wide spiral eddies classified into two subsidiary classes (disturbance and double helix). The central dye filament moves axially toward the orifice resistance aisles with a cylindrical section as illustrated in Figure-9, **(A)** without deviation, if for the vane, radially, $\Phi = 0$. Since the eddy/bubble transported gradually in the fluid, the focal dye filament has shown a small pulse in the filament within its end, whereas, if the swirl increased further than the reference value, as illustrated in dashboards (1,2) of Figure-18, the central filament (eddies class) moves gently and distinctly off-axis at azimuthal axis.

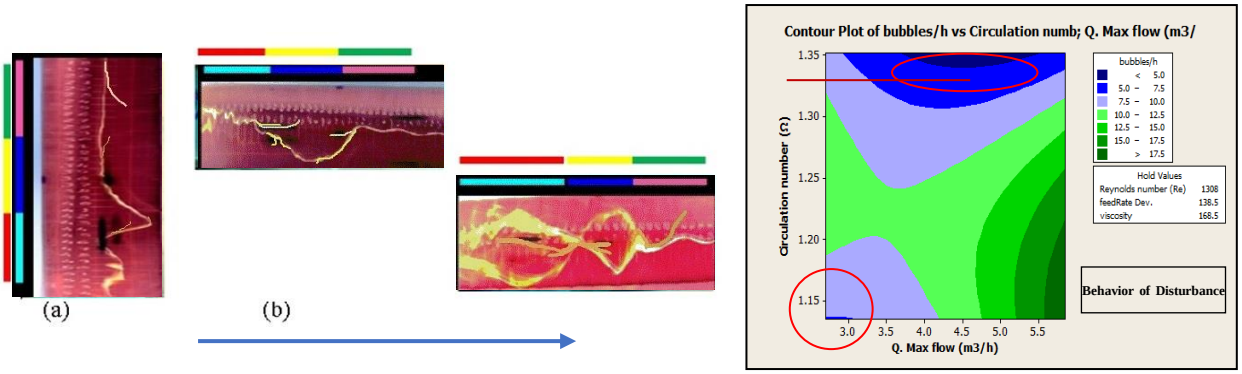

Db. (1) Type 1 **disturbance bubbles.**
(a) For (*Re* = 1308, **Ω** = 1.15)
(b) For (*Re* =1308, **Ω** = 1.32)

Db. (2) The disturbances of double helix waste.
(*Re* = 1500, **Ω** = 1.896)

Figure 18: (**a**) Type 1, The Db (1) and the Db (2) of wide spiral waste shape; (**b**) Type 1, The Db (2) of wide spiral bubble waste shape behavior.

According to the recorded observations, a wide spiral eddies (i.e., type 1) is controlled at (*Re*) ranging from 1308 to 1954 for cylindrical resistance aisles, which is illustrated in the dashboards (1 a & b) and dashboard (2), where the maximum direct flow is proportional with **Ω**. In both cases illustrated in the dashboards (1, 2) of type 1, the flow abruptly began to roll up, back toward the initial point of deviation, into a spiral. As this occurred, the filament downstream totally burst and create negative pressure pushes the air to high compliance room of ventilator through orifice resistance aisles, where (*Re*) =670 with **Ω** = 1.1800 to cause lung work.

5.1.1.2. Type 2.1, Flattened bubble eddies

The flattened eddies originated when type-1 disruption done, occasionally and spontaneously when the Reynolds numbers increased and Circulation decreased to control their paths toward resistance orifice and burst before pass to high compliance room. Therefore, the orifice prefered to be cone section as illustrated in Figure-9, **(B)** and analyzed at Figure-19, this transformation increase in the swirl, which undesirable. Therefore, The NN intervenes to prevent this transformation to control the propagation during fluid flow toward its destination (i.e., resistance compliance orifice room).

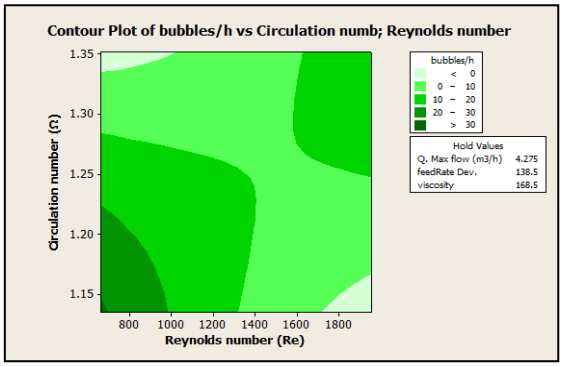

Figure-19: The relationship between Ω and (Re) to control the bubbles path

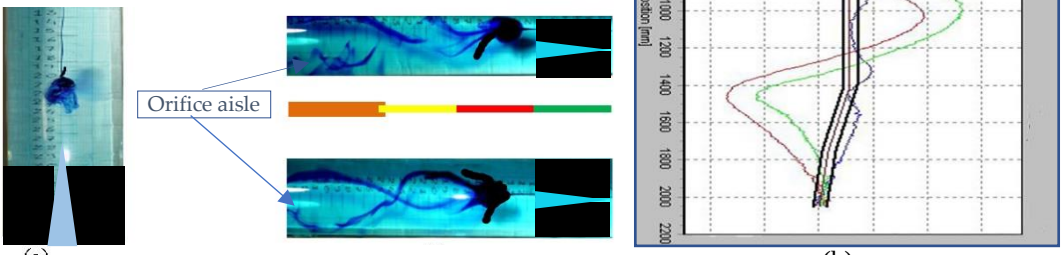

Db. (3) The flattened bubble eddies created instantaneously. ((Re) = 850, Ω = 1.31).

Dbs. (4 a & b) A flattened bubble eddies with several distinct empting ((Re) = 1850, Ω = 1.15).

Figure-20: (**a**) Type 2, The Db (3) and the Db (4a & 4b) of Flattened bubble waste shape; (**b**) Type 2, The Db (3) and the Db (4a & 4b) of Flattened bubble waste behavior.

5.1.1.3. Type 2.2, Bubble axially eddies

Figure-20, Db. (3) illustrates the birth of the flattened eddies, which in few seconds fully formed as dye began to exit from its tornado zone randomly and fail in passing through resistance orifice aisle toward high compliance room as illustrated in Figure-20 unless design this orifice in cone section and adjust the Re and Ω as illustrated in Dbs. (4 a and b). The Axial eddies class appeared intensively over the length of Db. (5) as illustrated in Figure-21, with an open and asymmetric rear, but have a short lifetime.

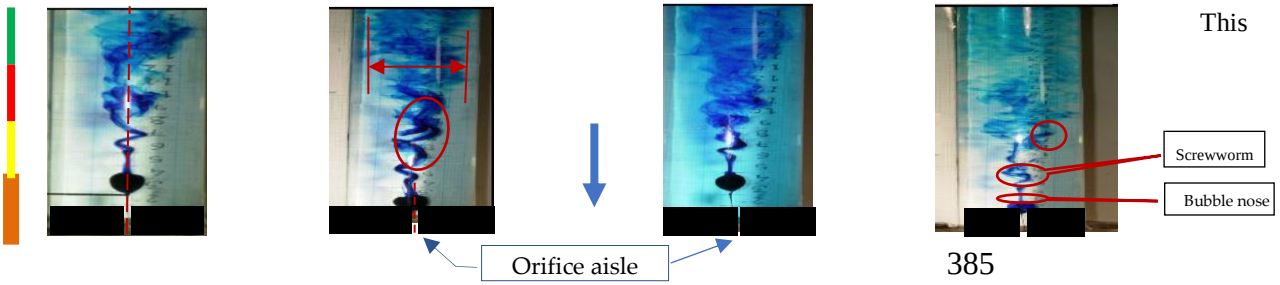

Db. (5) The axially eddy burst bubbles at (Ω =1.09 , 1600< (Re)<1887).

Db. (6 a) The wake instability for filling & emptying of the eddy and bubbles. (Ω = 1.17, 1600<(Re) <1885)

Db. (6 b) The emptying tail of the burst tended to return to the hose axis. (Ω = 1.26, (Re) = 1500).

Db. (6 c) The spiraling of the eddy core in bubbles (Ω = 2.25 , (Re) = 1954).

Figure-21: "The Bubble eddy axially image at different range of (*Re*) and Ω"

Therefore, must pass the resistance aisle orifice quickly via parabolic nose cone section. It is approximately one bubble in length leading to a loosely spiral eddies, which increases the likelihood of instabilities, especially if another bubble is formed uncontrollable turbulence. Indeed, eddies were spotted to fill and empty the route in two aspects: occurred at the fully obverse location near the backward of the eddy at one azimuthal axis, while it emptied at the azimuthal axis on the other side, 180º away, as illustrated in Db. (6 a) for 1600<(*Re*) <1885 and **Ω** = 1.17 at Figure-21. Eddies has an axial class because a stagnation point characterizes it, but soon the dye filament expanded to form the envelope of a bubble of the tornado. Therefore, the resistance room orifice must wide and short. But soon, its destination being filled and tilted toward the burst at the point farthest from its source and near the farthest destination point, but the generated pressure is weak, as discussed from Db. (6 b), while (Re) = 1500 and **Ω** = 1.26. These eddies of filling and discharging were the most commonly spotted one. The second eddies observed as illustrated in Db. (6 c), for (Re) = 1954 and **Ω** = 2.25, when the eddy has the tentative occurrence as a string on the axis inside bolt worm that preserved until the incubator exhaust all used liquid. Therefore, the incubator dispersed via a route far away from the related Reynolds (Re) = 1308 and Circulation **Ω** = 1.244 as inferred when controlling according to values shown in Figure-22.

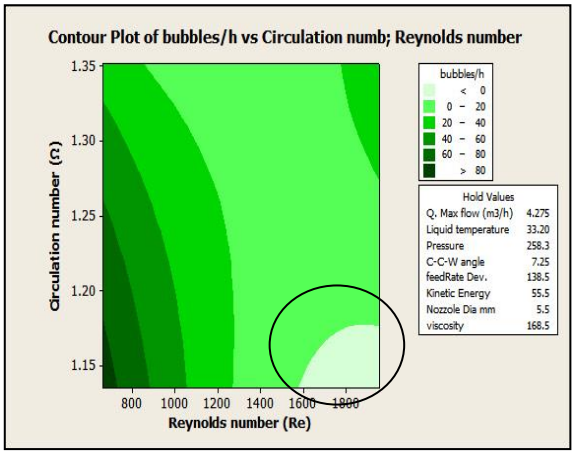

Figure-22: "Type 2, Flattened eddy's bubble affect according to Re and **Ω**"

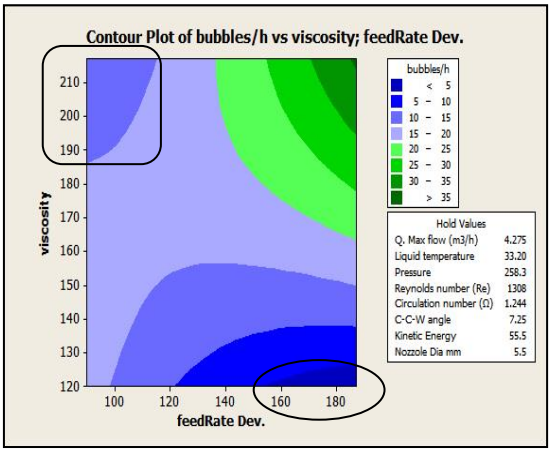

Figure-23: "Type 2, Flattened eddy's bubble affect according to viscosity and feed-rate"

6. Improvement phase

In this phase, we concentrated on constructing a new paradigm by using the Neural-Network learning and profoundly understand the ventilator operation unseen messages (Srikanth Namuduri, et al., 2020) between the collected data of the significant factors illustrated in Figure-14. This enabled us to make an intelligent type of ventilator incubator, and prelude to the control phase, where the device amended their entries (i.e., input significant factors) and adjusted their components' values to control the studied eddies as aforementioned (e.g., eddy creation, eddy movement, the underutilization). The ventilator operations has two modes of treatment. The first named the non-invasive ventilation (NIV), which follows two theories, PEEP vs. EPAP. The PEEP means Positive End-Expiratory Pressure, while EPAP means expiratory positive airway pressure; both based on tackling the patient's case via pushing air for inspiration for a fixed time ***(t)*** and then left the expiration process done automatically maybe for twice ***(t)*** mechanically without the slightest patients' help. The pressure may increase above the atmospheric one via liquid's incubator control as illustrates in Figure-23, and which points to the influencing of respiratory mechanism time. The second treatment named the continuous positive airway pressure (CPAP) based on drawing negative pressure as illustrates in Figure-24, via bursting eddies when paths through orifice resistance aisles when directs to high compliance room that mimics alveoli and back to zero in exhalation process, which determined via patient's lung ability to adjust the beginning pressure value. This pressure controlled via using IoT that contains a patient's data that analyzed and predicted the deviation of related influencing factors via NN to maintain the patient's stability case. The two treatments work under fixed 5cm H_2O pressure, which must be controlled.

The ventilator mechanism enhanced when its performance based on varying between NIV (PEEP or EPAP) at first and switch to CPAP to enhance the lung efficiency. Figure-17 aforementioned illustrates this switching through incubator (e.g., reservoir) appeared in **(D)** letter, which necessary controlled via adopting WPY to enhance its mechanism efficiency. The main target of WPY using is for monitoring the respiratory cycle time that shown in Figure-25 and illustrate that there are a time gap between the inspiration and expiration phases. The cycle-time is a summation of inhalation time **(T_I) (PEEP/EPAP)**, Pause phase (**T_{IPause}**) **(CPAP)**, and exhalation time **(T_E)**. These variables that measured via IoT data sensors and reserved on patient's dataset have been tackled through Neural-Network model to predict with its variation with time.

6.1. Neural-Network Model

Neural networks have been used with computers since the 1950s, and soon it became a tool used by all researchers from various disciplines who present many different models that specifically tailored for the deterministic cases. The perceptron is one of the earliest neural networks mimic a human memory, learning, and cognitive processes "human-like thought". Rather, the individual cells that make up the human brain are studied (JürgenSchmidhuber, et al., 2015). The human brain as a whole is far too complex to model aims at predicting the rapid deviation for some of the influencing factors affect for patients' cases and ventilators' performance. The data input for controlling the eddy/bubble-creating significant factors are feed-rate, viscosity, (*Re*), Ω, Ø muzzle orifice, and liquid temperature. These variables have correlation of 0.94 with the significant factors in causing defective behavior for the respiratory mechanism (which include pressure, Ø muzzle, respiratory cycle-time, (Re), Ω, and kinetic viscosity and vane angle) and considered the influencing inputs of neural structure as illustrated in Figure-26. The NN model consisted from 713 observations, and 72 of them used for training model proposed via the following code. Figure-27 clarifies the actual value vs. output plot for the trained ANN simulated by all the training data set. Performance of the network improved if the amount of training data increased, where the authors suffered in collecting the data effectively, where it collected in a mechanism environment, rather than a laboratory environment. This figure pushes to adjust the sensitivity of proposed smart ventilator device

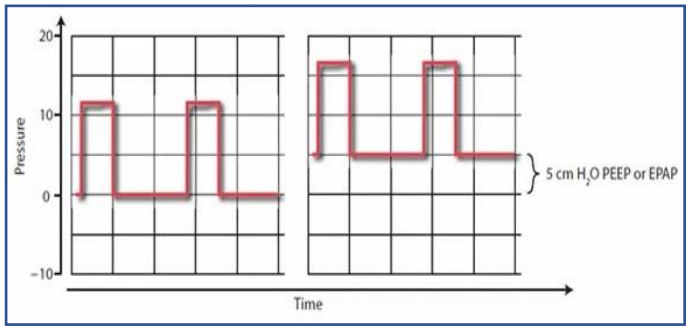

Figure-24: The upper airway profile pressure NIV

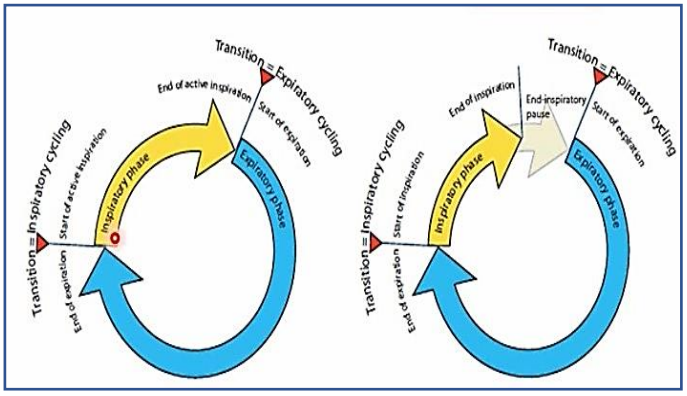

Figure-25: The respiratory cycle time

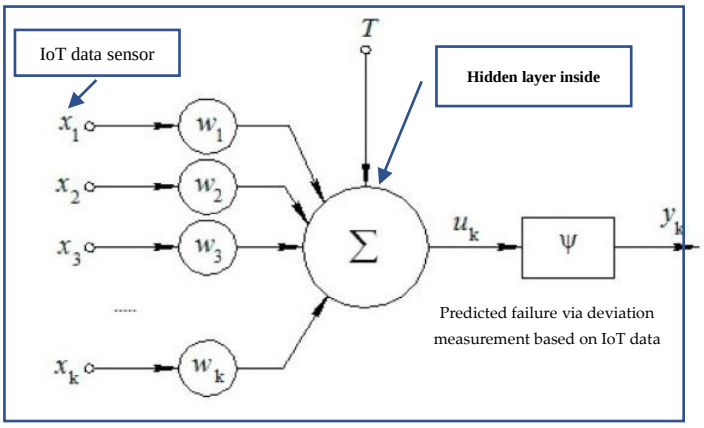

Figure-26: The structure of the neural element

adaptation every 15 sec, via adjusting the diameter of aisle's orifice.

```
close all, clear all, clc, format compact;
load Minitab_InputInfelunceVariables.mat
whos
figure
plot(EddyImage.Diameter(find(target==1),:)','b')
grid on, hold on
plot(Diameter(find(target>1),:)','r')
xabel('PassTime')        ylabel('Diameter')
[pn,ps1] = mapstd(Diameter');
FP.maxfrac = 0.05; [DetectEddy,ps2] = DetectEddy(pn,
FP);
EddyImage.Diameter2 = DetectEddy';
whosDiam. Diameter2
plot(EddyImage.diameter2(:,1),
EddyImage.diameter2(:,2),'.')
grid on, hold on
plot(EddyImage.Diameter2(find(target>1),1), Diameter2…
(find(target>1),2),'r.') xlabel('Time in sec')
ylabel('Orifice's aisle diameter')
target = double (target > 1);
net = feedforwardnet([6 4]);
net.divideParam.trainRatio = 0.70;
net.divideParam.valRatio = 0.15;
net.divideParam.testRatio = 0.15;
[net,tr,Y,E] = train(net,
EddyImage.Diameter2',target');
threshold = 0.5; Y = double(Y > threshold)';
cc = 100*length(find(Y==target))/length(target);
figure(28)
a = axis; xspan = a(1)-10 : .1 : a(2)+10; yspan = a(3)-
10 : .1 : a(4)+10;
[P1,P2] = meshgrid(xspan,yspan);
pp = [P1(:) P2(:)]';
aa = sim(net,pp);              aa = double(aa >
threshold);
ma = mesh(P1,P2,reclass(-
aa,length(yspan),length(xspan))-4);
mb = mesh(P1,P2,reclass(
aa,length(yspan),length(xspan))-5);
set(ma,'facecolor',[.7 1.0 1],'linestyle','none');
set(mb,'facecolor',[1 0.7 1],'linestyle','none');view(2)
```

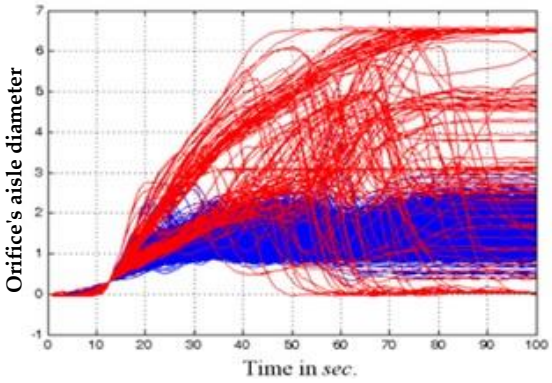

Figure-27: The time-distance eddy relationship

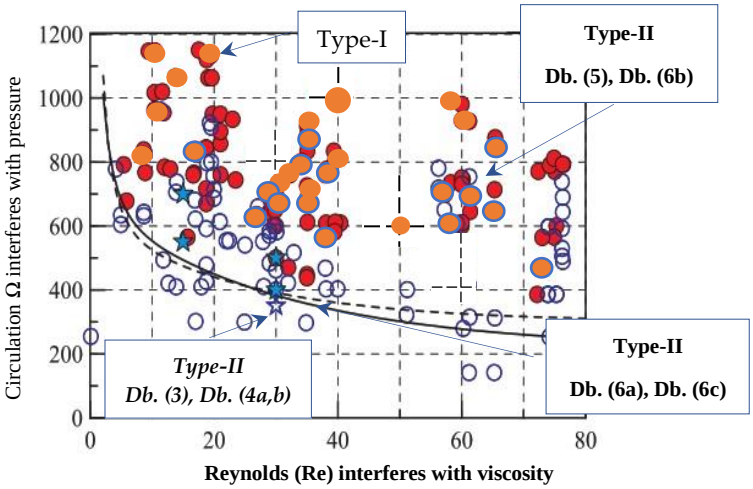

Figure 28: The intersection of significant factors

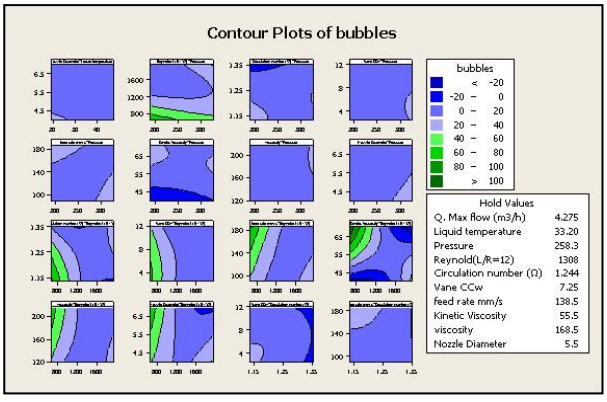

Figure-29: "The contour plots of bubbles creation causes as a beginning value of NN runs"

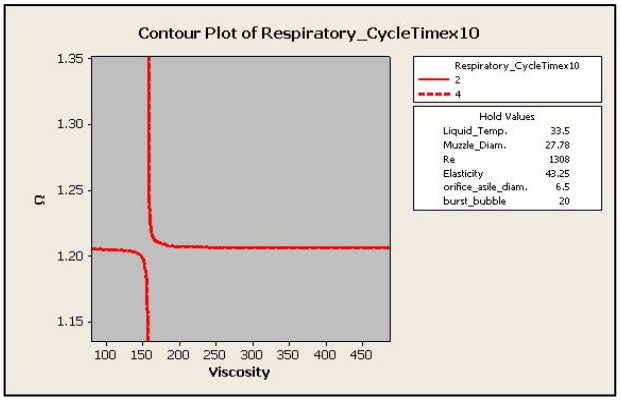

Figure-30: "The contour plots of respiratory cycle-time related with other influence variables"

This code's statements based on Neural-Network algorithm via back-propagation to reset all influencing inputs' data, as illustrated in [Figures 27, 28, 29 and 30]. The code optimizes the output of limited defects to gain six sigma standard values. Test Results; the results of testing for the ANN used in this work using unseen data are shown in Figure-31 for incubator (reservoir) capacity. The convergence condition considered when the range between actual values and predicted output is greater than 0.55, referred to as the limitation of training data set as illustrated in Figure-32.

6.2. The Wireless Poka-Yoke program code

This section of the paper will be using the so-called multilayer feed-forward network, which is the best choice for the proposed application. Each layer of the neural network contains connections to the next layer, which have the influencing variables, but there are no connections at backpropagation. Therefore, the proposed model illustrate in Figure-33 based on tackling the IoT data sensors that collect all measured values for patients' five cases and ventilators settings. One of the problems with the backpropagation training (i.e., it is a supervised learning method and is a generalization of the delta rule) is the degree to which the weights are changed. It requires a follower-up that knows or can calculate the desired output for any input in the training set [50]. In order to understand better the way error decreases and its rapid response time enhanced, consider the following error surface illustrates in Figure-34. Typically, the network consists of a set of sensory units (source nodes) that constitute the input layer, one or more hidden layers of computation nodes (i.e., unseen mechanism), and an output layer of computation nodes (i.e., pressure value). In its common use, most neural networks will have one hidden layer, and it's very rare for a neural network to have more than two hidden layers. The input signal propagates through the network in a forward direction, on a layer-by-layer basis. The proposed neural networks based on processing many variables in parallel at the same time commonly referred to as multilayer perceptron. Multilayer perceptron's have been applied successfully to solve some difficult and diverse problems, by training them in a supervised manner with a highly popular algorithm known as the error back-propagation algorithm (described further). Please note that in our application, we will be using the Resilient propagation algorithm, which is very similar to back-propagation [51]. The neural network itself will be composed of neurons (main information-processing units as neurons within a human brain) of the same kind, placed within different layers.

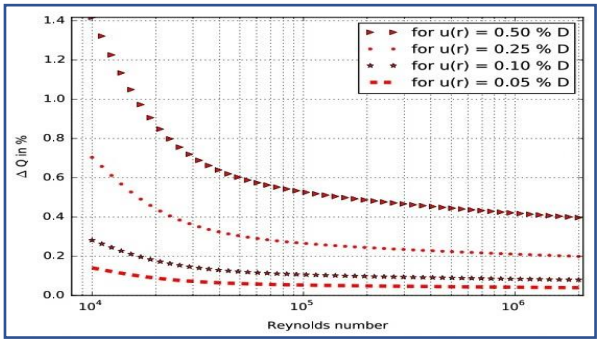

Figure-31: "Influence of the positional accuracy on the flow-rate velocity for Chebyshev method at (k=1)"

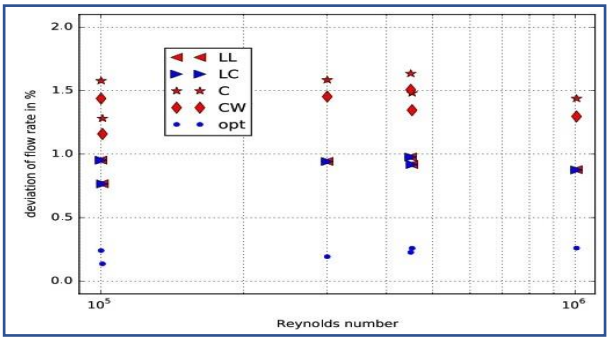

Figure-32: "Deviation of flow-rate through different velocity according to Reynolds (Re)"

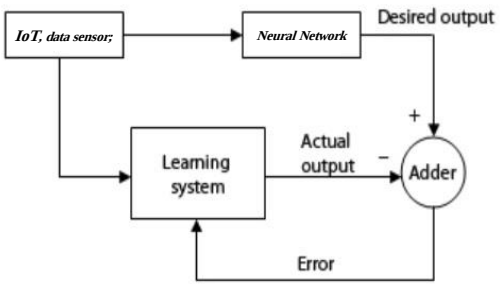

Figure-33: "The deep NN Resilient Back propagation model"

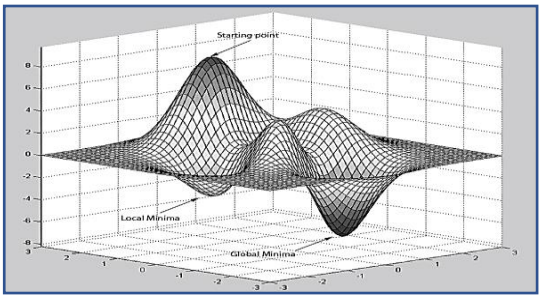

Figure-34: "The error surface for influence variables levels"

They will exhibit the same characteristics; hence, if you understand how one neuron designed you will not have problems in understanding how the entire network works. Generally, the model of a neuron can summarize in the following block diagram illustrated in Figure-35.

6.2.1. Pre-processing of the Eddies' Image

Imaging of eddies will be done in Grey-scaling after dye injection (i.e., each grayscale pixel value is divided by 256 to convert it to value ranging from 0 to1 so that it can be fed into a neural network) then shrinking the original image to 50x50 pixels will drastically reduce the number of input neurons to about 2500. This will also reduce the complexity and features that the neural network needs to analyze through the next code according to data shown in Table-2. This approach can be scaled to any number of classifications.

Table 2. Limit of input variables in the neural network model

Parameters		Down	Up
X_1:	Neurons number	2	16
X_2:	Learning rate	0.01	0.4
X_3:	Training counter	200	2500
X_4:	Momentum constant	0.1	0.9
X_5:	Number of training runs	3	7

```
public static EddyImage<Gray, Byte>
    ConvertOriginalEddyImageToGrayScaleAndProcess(EddyImage<Bgr, Byte> orginalEddyImage)
{
    var grayScale = orginalEddyImage.Convert<Gray, Byte>( );
    return grayScale.Resize(50,50, Emgu.CV.CvEnum.Inter.Cubic, false);
}
public static double[ ] GetNetworkFeedArray(EddyImage<Gray, Byte> EddyImage)
{
    var EddyImageBytes = EddyImage.Bytes;
    double[ ] networkFeed = new double[EddyImageBytes.Count( )];
    for (int i = 0; i < EddyImageBytes.Length; i++)
    {
        networkFeed[i] = ((double)EddyImageBytes[i] / 256);
    }
    return networkFeed;
}
public (double[ ][ ], double[ ][ ])
GetBatchDataFromEddyImages(IPagedList<LocalEddyImage>
localEddyImages)
{
    var numberOfEddyImages = localEddyImages.Count;
    double[ ][ ] batchInputs = new double[numberOfEddyImages][ ];
    double[ ][ ] batchOutputs = new double[numberOfEddyImages][ ];
    foreach (int i in Enumerable.Range(0, numberOfEddyImages))
    {
        var currentLocalEddyImage = localEddyImages[i];
        (double[ ] normalizedEddyImageData, EddyImageType EddyImageType) =
                LocalEddyImage.GetImageInformationForNeuralNetwork(currentLocalEddyImage);
        batchInputs[i] = normalizedEddyImageData;
        batchOutputs[i] = new double[ ]
                { currentLocalEddyImage.EddyImageType == EddyImageType.Eddy ? 1 : 0,
                  currentLocalEddyImage.EddyImageType == EddyImageType.Eddy ? 0 : 1 };
    }
    return (batchInputs, batchOutputs);
}
private static bool DetectEddy(INeuralNetwork neuralNetwork, EddyImage<Gray, Byte> EddyImage)
{
    double[ ] networkFeed = LocalEddyImage.GetNetworkFeedArray(EddyImage);
    var networkOutput = neuralNetwork.GenerateOutput(networkFeed);
    var outputValue = networkOutput[0];
    var complementaryOutputValue = networkOutput[1];
    return outputValue > 0.98 && complementaryOutputValue < 0.02;
}
```

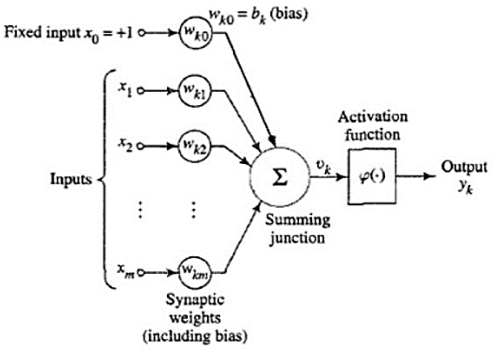

Figure-35: The Neuron's model block

It is important to remember that the inputs to the neural network model are floating-point numbers, which represented as C# double type. The output layer of the NN is what actually presents a pattern to the next mechanism stage. The number of output neurons related to the type of work that the NN is to perform. There are really two decisions that made regarding the hidden layers, which mimic the proposed mechanism: how many hidden layers actually have in the network and how many neurons will be in each of these layers. The answer based on the number of impact factors that must be tackled in parallel.

```
public static IncubatorSize GenerateNew( )
{
    double x = (random.NextDouble( )) / (double)1.1;   double y = (random.NextDouble( )) / (double)1.1;
    var smallerValue = x > y ? x : y;
    double width = random.Next(1000000, (int)(((double)1 - smallerValue) * 10000000)) / (double)10000000;
    double height = width;
    return new IncubatorSize( )
    {
        X = x, Y = y,
        Width = width,
        Height = height
    };
}
public static List<IncubatorSize > GenerateRandomIncubatorSizees( )
{
    var IncubatorSizeList = new List<IncubatorSize>( ) { new IncubatorSize( )
                    { Height = 1, Width = 1, X = 0, Y = 0 } };
    foreach (int i in Enumerable.Range(0, 1000))
    {
        IncubatorSizeList.Add(IncubatorSize.GenerateNew( ));
    }
    return IncubatorSizeList;
}
private static (EddyImage<Gray, Byte>, System.Drawing.Rectangle)
    GetAreaUnderIncubatorSize(EddyImage<Bgr, Byte> originalEddyImage, IncubatorSize IncubatorSize)
{
    var originalEddyImageCopy = originalEddyImage.Copy( );
    var rectangle = GetRectangleFromAnchroBox(originalEddyImageCopy, IncubatorSize);
    originalEddyImageCopy.ROI = rectangle;
    var croppedEddyImage = LocalEddyImage.ConvertOriginalEddyImageToGrayScaleAndProcess (originalEddyImageCopy.Copy( ));
    originalEddyImageCopy.ROI = System.Drawing.Rectangle.Empty;
   return (croppedEddyImage, rectangle);
}
private CPAPBeliveNetworkLearning
      GetUnsupervisedTeacherForNetwork(CPAPBeliveNetwork CPAPNetwork)
{
    var teacher = new CPAPBeliveNetworkLearning(CPAPNetwork)
    {
        Algorithm = (hiddenLayer, visibleLayer, i) => new ContrastiveDivergenceLearning(hiddenLayer, visibleLayer)
        {
            LearningRate = 0.1,
           Momentum = 0.5
        }
    };
    return teacher;
}
private ResilientBackpropagationLearning GetSupervisedTeacherForNetwork (CPAPBeliveNetwork CPAPNetwork)
{
    var teacher = new ResilientBackpropagationLearning(CPAPNetwork)
    {
        LearningRate = 0.1 //Momentum = 0.5
    };
    return teacher;}
```

6.2.2. Training Code to activate the WPY model

```
/// <summary>// Train network/// </summary>
/// <param name="status">Delegate to be invoked</param>
/// <param name="trainFrom">Train from</param>
/// <param name="trainTo">Train to</param>
private void TrainNetwork(DateTime trainFrom, DateTime trainTo, TrainingStatus status)
{
    if (_input == null || _ideal == null)
        CreateTrainingSets(trainFrom, trainTo); /*Create training sets, according to input parameters*/
    _trainThread = Thread.CurrentThread;
    int counter = 1;
    ITrain train = null;
    try
    {
        /*Start training with Resilient-backpropagation algorithm*/
        var trainSet = new BasicNeuralDataSet(_input, _ideal);
        train = new ResilientPropagation(_network, trainSet);
        double deviation;
        do
        {
            train.Iteration( );
            deviation = train.Deviation;
            if (status != null)
                status.Invoke(counter, deviation, TrainingAlgorithm.Resilient);
            counter++;
        } while (deviation > MaxDeviation);
    }
    catch (ThreadAbortException) {/*Training aborted*/_trainThread = null; }
    finally
    {
        train.FinishTraining( );
    }
    _trainThread = null;
}
/// <summary>/// Create a new network/// </summary>
/// <param name="unseenMechaneism">Number of hidden layers</param>
/// <param name="hiddenUnits">Number of hidden units within each hidden layer</param>
private void CreateNetwork(int hiddenUnits, int unseenMechaneism)
{
    _network = new BasicNetwork {Name = "Eddies path Predictor",
            Type = "Network for prediction analysis"};
    _network.AddLayer(new BasicLayer(INPUT_TUPLES * INDEXES_TO_CONSIDER)); /*Input*/
    for (int i = 0; i < unseenMechaneism; i++)
        _network.AddLayer(new BasicLayer
            (new ActivationTANH( ), true, hiddenUnits));
    _network.AddLayer(new BasicLayer (new ActivationTANH(), true, OUTPUT_SIZE));
    _network.Structure.FinalizeStructure( );
    _network.Reset( );
}
```

7.1. Output analysis

Calculating the output of a single image input, which appeared in dashboards from (1) to (6), are analyzed in a single line. The length of the output array is the same as the number of output neurons in the network. There are five types (A, B, C, D, and E) of patients' cases as illustrates in Figure-36 that must proposed code guarantee the rapid response to reduce the risk and increase the ventilator's performance. This code activate the aforementioned the resilient back propagation model to enhance the data collected to predict the most suitable case of ventilator adjustable to reduce patient's risk.

```
public double[ ] GenerateOutput(double[ ] inputs)
{
Switch (infeluncing_factors)
Infeluncing factors == respiration cycle-time
Case mandatory_inspiration_A:
Push_high_rate_air ON;
```

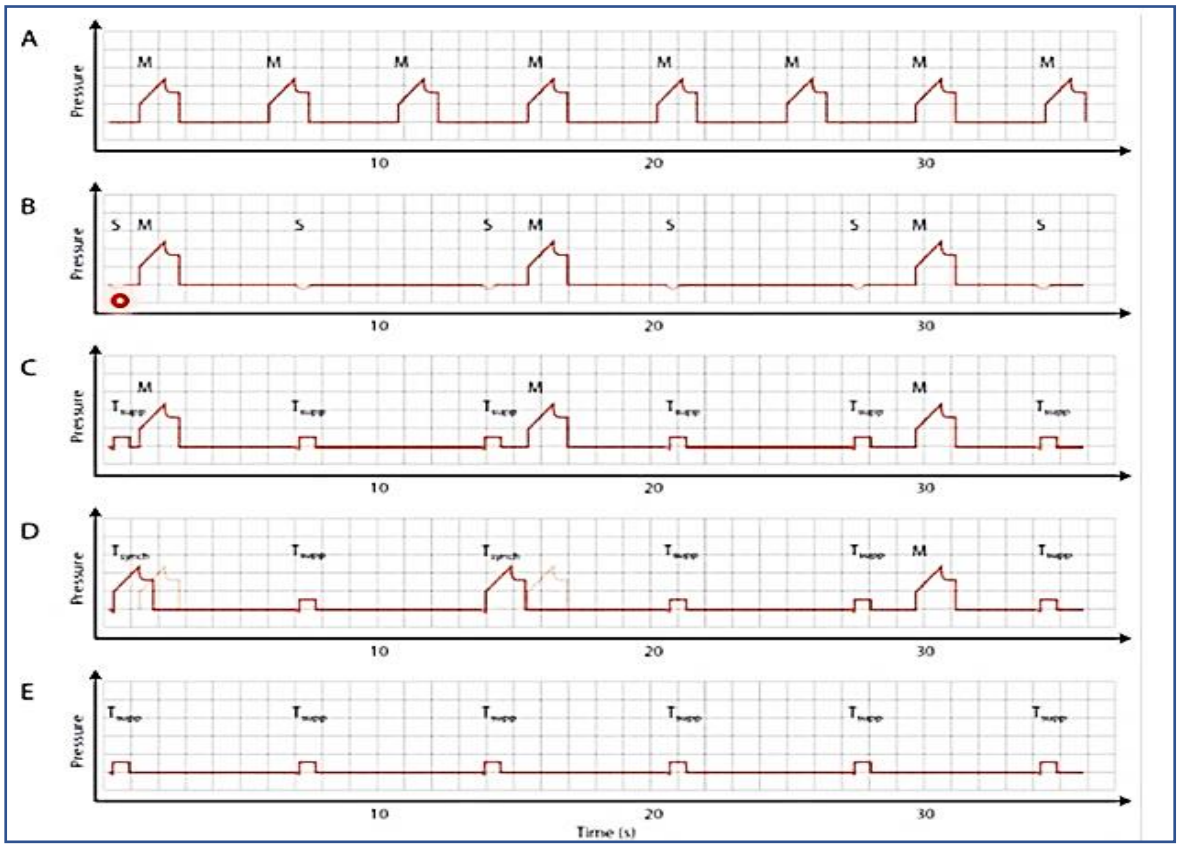

Figure-36: The most common patients' cases when use ventilator device

Db. (1, a)

Patient's case		Ventilator adjustment	
Unexplained hyperthermia	38.5 ^{0}C	**Temperature**	33 ^{0}C
		Viscosity	1.31 mPa s
Hyper-Coagulable	Low	**Reynolds Number**	1308
		Circulation No.	1.15
Respiratory acceleration	Low 7/minute	**Respiratory cycle time**	3.12 sec
		Orifice aisle section	Cylinder

Db. (1, b)

Patient case		Ventilator adjustment	
Unexplained hyperthermia	38.5 ^{0}C	**Temperature**	33 ^{0}C
		Viscosity	0.931 mPa s
Hyper-Coagulable	Low	**Reynolds Number**	1308
		Circulation Number	1.32
Respiratory acceleration	High 15/minute	**Respiratory cycle time**	3.12 sec
		Orifice aisle section	Cone

```
Break;
Case spontaneous_ inspiration_B:
Push_low_rate_air ON;
```

Db. (2)

Patient's case		Ventilator adjustment	
Unexplained hyperthermia	39 ^{0}C	**Temperature**	34 ^{0}C
		Viscosity	0.931 mPa s
Hyper-Coagulable	Moderate	**Reynolds Number**	1500
		Circulation Number	1.896
Respiratory acceleration	Low 7/minute	**Respiratory cycle time**	3.62 sec
		Orifice aisle section	Cylinder

```
Break;
```

713 ***Case** spontaneous_ inspiration_C:*
714 ***If** $\Delta C_{lung} > \Delta C_{capillary}$;*
715 ***Mix Mandatory &spontaneous air ON;***
716 ***Push_low_rate_air_with_low_pressure ON;***

Db. (3)

Patient's case		Ventilator adjustment	
Unexplained hyperthermia	39 ^{0}**C**	**Temperature**	34 ^{0}**C**
		Viscosity	1.01 mPa s
Hyper-Coagulable	moderate	**Reynolds Number**	850
		Circulation Number	1.31
Respiratory acceleration	High **15/minute**	**Respiratory cycle time**	4.12 sec
		Orifice aisle section	Cone

717 ***Break**;*
718 ***Case** sycronization_ inspiration_D:*
719 ***If** $\Delta C_{lung} < \Delta C_{capillary}$*
720 ***triggering_earlier_inspiration_action ON;***
721 ***make shift to left for distribution of case C;***

Db. (4, a)

Patient's case		Ventilator adjustment	
Unexplained hyperthermia	40 ^{0}**C**	**Temperature**	26 ^{0}**C**
		Viscosity	1.31 mPa s
Hyper-Coagulable	High	**Reynolds Number**	1850
		Circulation No.	1.15
Respiratory acceleration	Moderate **11/minute**	**Respiratory cycle time**	3.0 sec
		Orifice aisle section	cylinder

Db. (4, b)

Patient case		Ventilator adjustment	
Unexplained hyperthermia	40 ^{0}**C**	**Temperature**	29 ^{0}**C**
		Viscosity	1.24 mPa s
Hyper-Coagulable	Low	**Reynolds Number**	1916
		Circulation Number	1.15
Respiratory acceleration	High **15/minute**	**Respiratory cycle time**	4.12 sec
		Orifice aisle section	Cone

722 ***Else***

Db. (5)

Patient's case		Ventilator adjustment	
Unexplained hyperthermia	40 ^{0}**C**	**Temperature**	37 ^{0}**C**
		Viscosity	0.806 mPa s
Hyper-Coagulable	High	**Reynolds Number**	1600 : 1887
		Circulation Number	1.09
Respiratory acceleration	High **15/minute**	**Respiratory cycle time**	4.62 sec
		Orifice aisle section	parabolic nose cone

723 ***Break**;*
724 ***Case** Stop_ ventilation_effect_E:*
725 ***If** $\Delta C_{lung} == \Delta C_{capillary}$*

D(b. 6,a)

Patient's case		Ventilator adjustment	
Unexplained hyperthermia	39 ^{0}**C**	**Temperature**	37 ^{0}**C**
		Viscosity	0.735 mPa s
Hyper-Coagulable	High	**Reynolds Number**	1600 : 1885
		Circulation Number	1.17
Respiratory acceleration	Low **5/minute**	**Respiratory cycle time**	2.82 sec
		Orifice aisle section	Cone

Db. (6,b)

Patient's case		Ventilator adjustment	
Unexplained hyperthermia	40.5 ^{0}**C**	**Temperature**	35 ^{0}**C**
		Viscosity	0.891 mPa s
Hyper-Coagulable	moderate	**Reynolds Number**	1500
		Circulation Number	1.26
Respiratory acceleration	moderate **10/minute**	**Respiratory cycle time**	3.12 sec
		Orifice aisle section	cylinder

Db. (6,c)

Patient's case		Ventilator adjustment	
Unexplained hyperthermia	42 ^{0}**C**	**Temperature**	34 ^{0}**C**
		Viscosity	0.781 mPa s
Hyper-Coagulable	Low	**Reynolds Number**	1954
		Circulation Number	2.25
Respiratory acceleration	High **16/minute**	**Respiratory cycle time**	4.12 sec
		Orifice aisle section	parabolic nose cone

726 ***Break;***

```
Default
 return network.Compute(inputInfeluenceVariables);
}
```

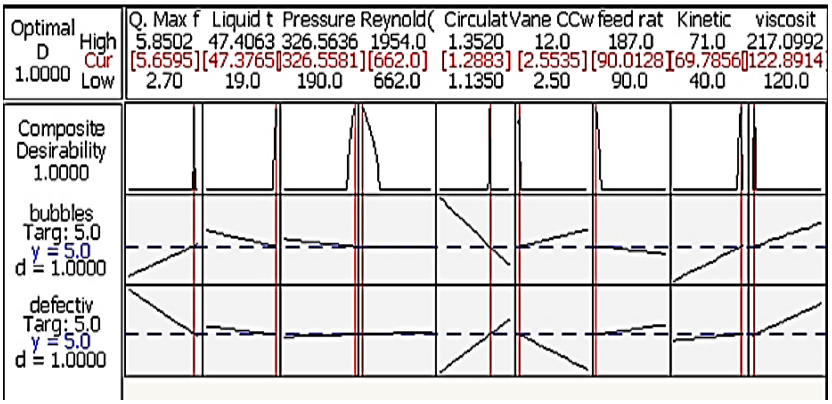

Figure-37: "Optimum value of influence factors to control eddies paths to rapid response time in pushing suitable air pressure"

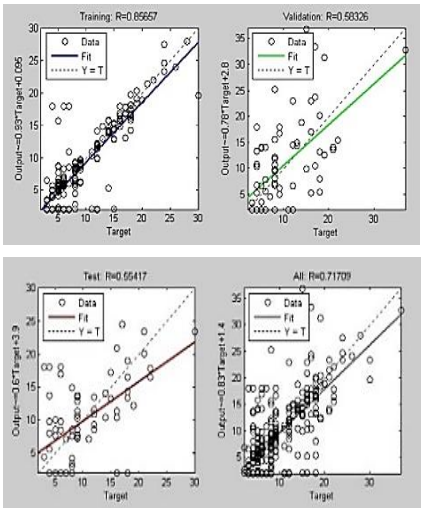

Figure-38: "The Neural-Network output performance"

7.2. Preliminary Results of eddies with reservoir (Incubator capacity) L/R = 12

The original disturbance location for all types of bubble eddies (i.e., movement) based on (Re) and Ω together. The disturbance class moved upstream as ((Re)) is increased and fixed (Ω), but if the imparted swirl that has been increased, then the flow moves at a fixed rate. Figure-37 illustrates the optimum values for all influencing factors affect incubator and patients' cases. Figure-38 illustrate the analysis of NN when use the optimal values shown in Figure-37 to test the ventilator performance to adjust patients' cases. The outcomes of the dimensionless eddies, normalized according to incubator (e.g., reservoir) capacity (radius and depth) taking into account $\psi+ = \psi/R = 0.6''$. The capacity effect on variables deviation for L/R =12 according to respiratory cycle-time, are plotted in Figure-39 vs. (Re) and eight different values of Ω, clockwise (because at Counter Clock Wise is optimized) flow direction (because it is significant).

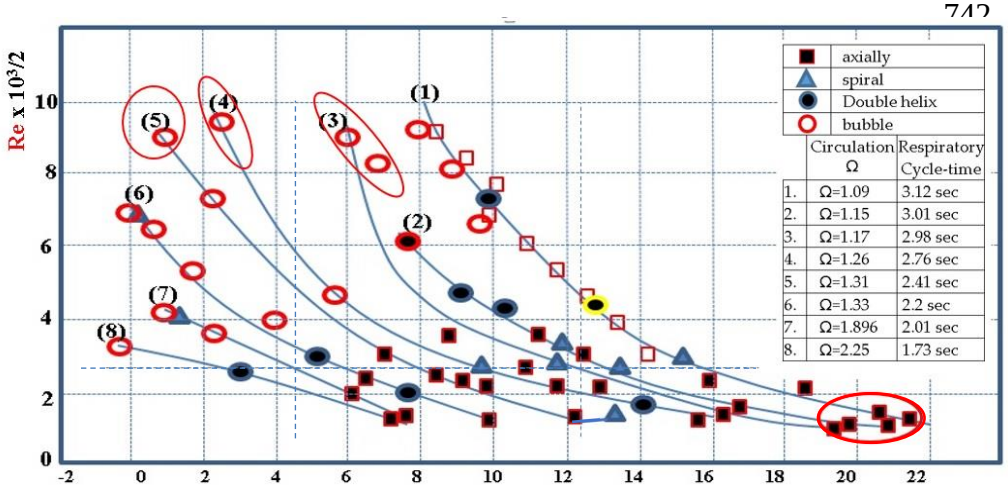

Figure-39: "Eddy burst as function of Re $_{and}$ Ω at clockwise flow direction for L/R = 12"

Figure-39 illustrates that at Ω = 1.32 and (Re) = 1384, the disturbance was found to be a wide spiral (type 1) at a distance of about ψ+ = 10.5, point (a). When (Re) was increased to 1888 the type (1) was still occurring but the

disturbance moved upward to a new eddies of ψ+ = 9.6 point (b). The reliability of the process increases with NN intervention, reducing the responding time to adjust its influencing factors to increase WPY efficiency by 99.8%, by reducing the number of slowdown and rapid response time from 70 sec to 3 sec. The respiratory cycle-time is inversely related with circulation value that controlled according to patient's cases that illustrated in Figure-36.

8. Control Phase

In the final phase, it should be borne in mind that wide variation in viscosity value of patient might lead to serious consequences, despite the viscosity not being one of the common significant factors according to the control of Figures 29 and 30. Therefore, it recommended fixing it at 168.56 *mPa* throughout the control phase, which revealed that there are three distinct eddies moving toward orifice of resistance high compliance room (i.e., mimicked alveoli) that affected by significant factors such as (Re), feed-rate, viscosity, and Ω, which are varied to generate pressure pushes the air. Two of these eddies (wide spiral and flattened bubble) occurred at (Re) from 670 to 1954 for L/R = 12. Therefore, the NN used to avoid the occurrence of these types via controlling the optimized values. The other type of eddies occurred at the highest values of (Re) and was defined by axial eddies' bubble based on circulation; Ω. Eddies appeared in the hysteresis zone occasionally, shriveling in size (i.e., both diameter and length) as the (Re) or Ω is increased. The liquid temperature was set at 47 ° C, whereas the ambient temperature adapted to room temperature.

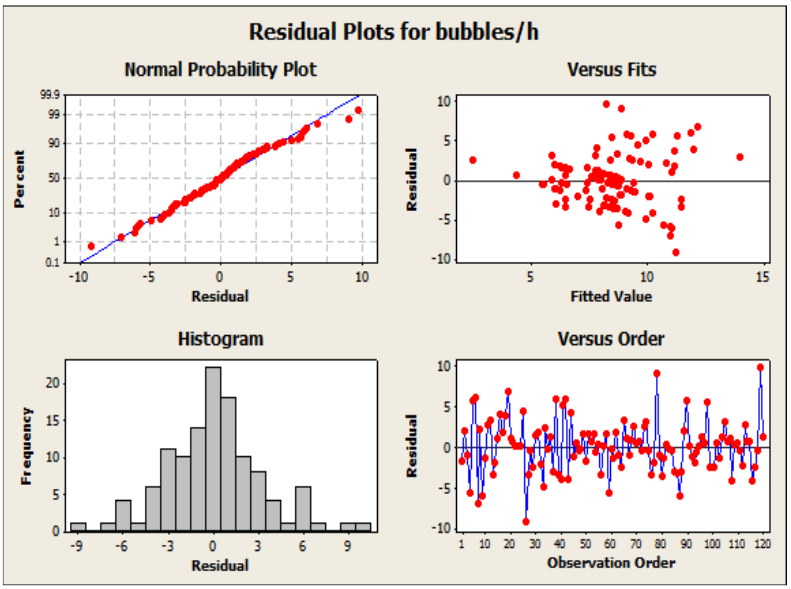

Figure-40: "Residual Plots for bubbles' eddy /h"

The results of the experimental study drawn from the swirled flow through circular straight reservoir (i.e., Incubator) as follows:

1) The eddy creation bubbles are smaller for the anti-clockwise special flow direction under control, especially when pass the cylindrical orifice (L/R = 12). Therefore, to control the output of process performance must follow Figure-40 recommendations.

2) Eddies' movement path directions were based on both the (Re) and Ω of the incubator's liquid. However, for some (Re) values increasing Ω always lead to pushing eddies downstream toward the destination point via orifice of resistance room. In contrast, an increase in Ω leads to a transformation to another type of eddies class. The direction of the bubble's burst movement is also resulted generally, when (Re) increased at a constant value of Ω, viscosity and temperature. This profile is more suitable for patients' cases A, C.

3) In state of Ω = 1.186, a small influence of the eddy bubble can be noted for the cylindrical orifice for the resistance aisle with the anti-clockwise vane of flow direction and set at approximately 12o. This profile is more suitable for patients' cases B, C. There is no significant for Hyper-Coagulable level.

4) In case of anti-clockwise flow direction, the eddy always occurred at the destination of the orifice of parabolic nose cone rather than that in the cylindrical orifice section for all values of Ω, except when Ω ≥ 1.6, where the eddy has a small effect. This profile is more suitable for patients' case C.

5) On the other hand, in the clockwise flow direction case, the bubbles' eddy occurs at the end of the cone orifice more than in parabolic nose cone at Ω =1.28, but the results change when Ω is increased to 1.6, where the bubbles' eddy pass quickly in the parabolic nose cone than about it in the cylindrical one and create negative pressure enough to lung trigger. This profile is more suitable for patients' cases C, D.

6) The eddy moves slowly toward injection arm at the anti-clockwise flow case for some of the optimal values for the influencing factors, whereas the circulation of Ω increases, whether for cone or cylindrical orifice travel.

7) The reliability of the process increases with NN intervention, reducing the defective output by 92.8%, by reducing the number of defective bathtubs from 70/week to 5/week.

9. Conclusion

The proposed NN model which based on IoT data that begins it's predicting for process deviation from optimum of significant local values illustrated in Figure-16, which generated by DOE. The proposed model achieves approximately an accuracy of 98.6% in responding-time rapidly and adjusts its inputs according to patients' cases. This work based on the imaging processes' mechanism through monitoring eddies that occur and follow its paths profoundly to enhance the ventilator work and increase its sensitivity to reduce the risky situation when respiratory cycle-time became not suit the patient's case according to Figure-41. Therefore, this work proposes a novel approach called a WPY, which derivative from DMAIC tools used to fool-proofing action. This work follows some of eddies' aspects that created to push their bubbles toward high compliance room orifice, which mimic alveoli when receiving the air. The study aims at monitors eddies' paths to install orifice of proposed resistance aisles in face of these paths with different sections varied according to eddies type. This approach controlled through IoT data and begins with determine all influencing factors that effect on the outputs' pressure as illustrates in Figure-42, then collects the statistical data for eddies types by imaging process and follow their paths to control them and enhance the results via using NN. This model aims at rapid response time of ventilator and patients' cases remotely, that named wireless poka-yoke "WPY". The WPY based on any of optimization models to control eddies' path to push maximum number of bubbles toward the balloons (i.e., alveoli mimicker) through orifice aisles and create negative pressure pushing the air to working lung according to the patients' biological factors. This work adopts the neural networks that based on IoT data sensor to predict the optimum values for the significant variables that selected from applying full factorial DOE, for more details about IoT, ensemble models, refer to V. T. Tran, et al., 2012 and J. Steinbock, et al., 2016 respectively. If these values controlled via machine (e.g., ventilator or equipment), which giving it new name (e.g., smart machine), because it resists eddies causes to control

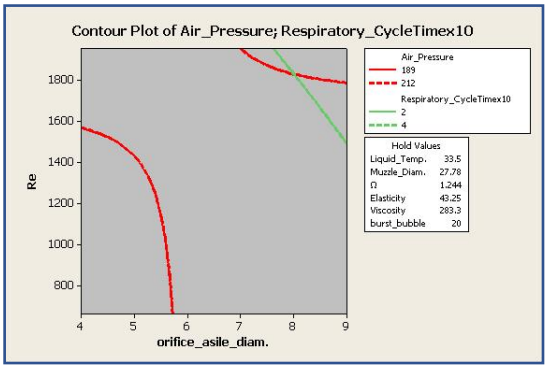

Figure-41: "Respiratory cycle-time affected by pressure under other influence factors"

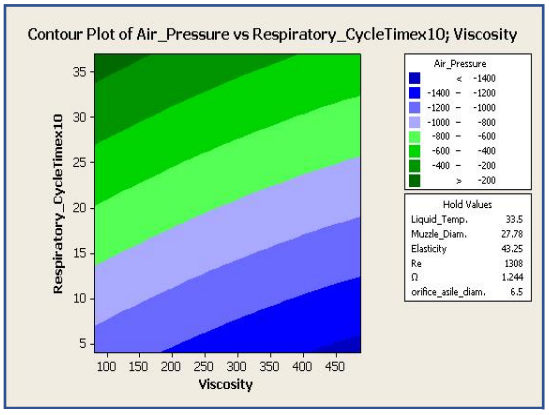

Figure-42: "Respiratory cycle-time related with viscosity"

losses costs. All setting variables for these specific processes case listed in control phase section 8. The slowdown ventilator reduced to less than 0.08% via join its mechanism with IoT that enhanced with NN model that control all of its impact input variables that represent influencing factors only x_i.

Author Contributions: Conceptualization, A.A.; Methodology, A.A and T.G.; Software, T.G.; Validation, A.A; and T.G; Formal Control, A.A.; Investigation, A.A. and T.G.; Resources, A.A.; Data Curation, A.A. and T.G.; Writing-Original Draft Preparation, A.A.; Writing-Review & Editing, T.G.; Visualization, A.A. and T.G.; Supervision, A.A.; Project Administration A.A.

Acknowledgments: This research was funded by Authors, whether for data collection, analysis, and evaluation through experimentation involving various groups of rabbits and dogs suffer from Shortness of breath.

Conflicts of Interest: The authors declare no conflict of interest.

References

Liu F., Jang H., Kijowski R., Bradshaw T., and McMillan AB., **2018**, "Deep learning MR imaging-based attenuation correction for PET/MR imaging". *Radiology*, 286, pp. 676–684.

Huang G., Liu Z., van der Maaten L., and Weinberger KQ., **2017**, "Densely connected convolutional Networks". *In: Proceedings of the 2017 IEEE Conference on Computer Vision and Pattern Recognition (CVPR)*. 2017. https://doi.org/10.1109/CVPR.2017.243.

Krizhevsky A, Sutskever I., and Hinton GE., **2012**, "Image Net classification with deep convolutional neural networks". *Adv Neural Inf Process Syst*, 25. Available online at: https://papers.nips.cc/paper/4824-imagenet-classification-with-deep-convolutional-neural-networks.pdf Accessed 22 Jan **2018**

Bastiaanssen WGM., Molden DJ., and Makin IW., **2000**, "Remote sensing for irrigated agriculture: examples from research and possible applications. *Agricultural* Water *Management*", 46, pp.137–155.

Gebbers R., and Adamchuk VI., **2010**, "Precision agriculture and food security". *Science*, 327, pp. 828–831.

Maria Joao Félix, Silvio Silva, Gilberto Santos, Manuel Doiro, José Carlos Sa., **2019**, "Integrated product and processes development in design: A case Study", 8th Mechanism Engineering Society International Conference, Procedia Mechanism 41 296–303, Available online at www.sciencedirect.com

M. Rükmann, M. Lorenz, P. Gerbert, M. Waldner, J. Justus, P. Engel, M. Harnisch, **2015**, "Industry 4.0: The future of productivity and growth in mechanism industries", Bost. Consult. Gr.; 9: 54–89.

G. Ringen, T. Welo., **2018**, "The product devel. learning process and its relation to performance indicators". Procedia Manuf.; 26: 107–116.

Weber RH., and Weber R., **2010**, "Internet of Things",12, New York, NY, USA: Springer.

Hashem IAT., Yaqoob I., Anuar NB., Mokhtar S., Gani A., and Khan S., **2015**, "The rise of 'big data' on cloud computing: review and open research issues*". Information Systems*, 47, pp. 98–115.

Chi M., Plaza A., Benediktsson JA., Sun Z., Shen J., and Zhu Y., **2016**, "Big data for remote sensing: challenges and opportunities". *Proceedings of the IEEE*,104, pp.2207–2219.

Kamilaris A., and Prenafeta-Boldú FX., **2017**, "Disaster monitoring using unmanned aerial vehicles and deep learning". *In Disaster Management for Resilience and Public Safety Workshop, Proceedings of EnviroInfo*. Luxembourg.

LeCun Y., Bengio Y., and Hinton G., **2015**, "Deep learning". *Nature*, 521, pp.436–444.

M. Gregor, J. Kosturiak J., **2017**, "Simulation: strategic technique for the Factory's future", Revue Simulation, 291-305.

Paloma Diaz-Guti_errez, Sam J. Gilbert, Juan E. Arco, Alberto Sobrado, Maria Ruz., **2020**, "Neural representation of current and intended task sets during sequential judgments on human faces", journal of NeuroImage, NeuroImage 204, 116219.

D.R. Kiran, "Business Process Reengineering". Total Quality Management, **2017**, pp. 405-414

875 Abed A., and Farag S., **2014**, "Control vortex Position in Vertical Tube to Reduce Spray Defects and Revamping Six-
876 Sigma Image Verification Tool". *The Egyptian Int. J. of Eng. Sci. and Technology* ,17, pp. 178-185.

877 Ioffe S., and Szegedy C., **2015**, "Batch normalization: accelerating deep network training by reducing internal
878 covariate shift". arXiv, Available online at: https://arxiv.org/pdf/1502.03167.pdf Accessed 22 Jan 2018.

879 Leibovich S., **1978**, Ann. Rev. of Fluid Mech.: The structure of vortex breakdown, Volume 10; pp. 221 – 246.
880 Peckham D., and Atkinsion S., **1957**, "Preliminary results of low speed wind tunnel tests on a gothic wing of aspect
881 ratio". 1.0. *ARC technical report* CP No.50.

882 Srigrarom S., and Ridzwan M., **2007**, "An experimental investigation of perturbations on vortex breakdown over delta
883 wings". *16th Australasian fluid mechanics conference Gold Coast Australia* (2-7 December 2007).

884 Srigrarom S., and Lewpiriyawong N., **2007**, "Controlled eddy breakdown on modified". *J. of Visulization*,10, pp. 299-
885 307.

886 Sharma C., Soundranayagam S., Mukund S., and Mukund T., **1998**, "Dependence of vortex breakdown on angular
887 momentum parameter in draft hose flows". *Current Science*, 75, pp.1355-1363.

888 Cervants M., **2009**, "Counter rotating runner cone in a Kaplan elbow draft hose for increased efficiency". *3rd IAHR*
889 *International meeting of the works group on cavitation and dynamic problems in hydraulic machinery and*
890 *systems* 14-16 Brno Czech Republic.

891 Tangermann E., and Pfitzner M., **2009**, "Evaluation of combustion models for combustion-induced vortex
892 breakdown". *Journal of Turbulence Taylor &* Francis.

893 Aksel M., and Kaya M., **1992**, "A numerical simulation of the axisymmetric vortex breakdown in a hose". *Applied*
894 *Mathematical modeling*, 16, pp. 414-422.

895 Jochmann P., Sinigersky A., Hehel M., Schäfer O., Koch R., and Bauer H., **2006**, "Numerical simulation of a
896 processing vortex breakdown". *International J. of Heat and Fluid Flow*, 27, pp. 192 – 203.

897 Harvey J., **2006**, "Control of the vortex breakdown phenomenon. Imperial Collage, Department of aeronautics",
898 Report No. 103.

899 P.J. Sousa, F. Barros, P. J. Tavares, **2017**, "Displacement measurement and class acquisition of an RC helicopter blade
900 using Digital Image", Correlation, Procedia Structural Integrity, 5, 1253–1259.

901 J. Park, S. Yoon, T.-H. Kwon, K. Park, **2017**, "Assessment of speckle-pattern quality in digital image correlation based
902 on gray intensity and speckle morphology", Optics and Lasers in Engineering, 91,62–72.

903 C. Bermudo, S. Martin-Béjar, F.J. Trujillo, G. Castillo, L. Sevilla, **2019**, "Material flow control in indentation process
904 by 3D Digital Image Correlation", 8th Mechanism Engineering Society International Conference, Procedia
905 Mechanism 41, 26–33, www.sciencedirect.com

906 Srikanth Namuduri, Barath Narayanan Narayanan, Venkata Salini, Priyamvada Davuluru, Lamar Burton, and Shekhar
907 Bhansali 2019 " Review—Deep Learning Methods for Sensor Based Predictive Maintenance and Future
908 Perspectives for Electromixture Sensors", Journal of The Electromixture Society, **2020** 167 037552

909 A.G.Arteaga, Roque Calvo., **2019**, " Experimental control of alternative production flow controls for high variety
910 product mechanism", 8th Mechanism Engineering Society International Conference, Procedia Mechanism 41,
911 249–256, www.sciencedirect.com

912 M. Fadzly, M. Saad, Z. Shayfull, "Control on Flexible Mechanism System Layout Using Arenas Simulation Software"
913 American Institute of Physics 3rd Electronic and Green Materials International Conference (**2017**).

914 Lucke, M., Mei, X., Stief, A., Chioua, M., & Thornhill, N. F. **2019**, "Variable selection for eddies detection and
915 identification based on mutual information of alarm series". In Proceedings of 12th DYCOPS symposium (pp.
916 673–678). Florianópolis, Brazil: http://dx.doi.org/10.1016/j.ifacol.2019.06.140, IFAC-PapersOnLine.

917 K. Chen, C.-C. Chang, **2019**, High-capacity reversible data hiding in encrypted images based on extended run-length
918 coding and block-based msb plane rearrangement, J. Vis. Commun. Image Represent. 58, 334–344.

Xiaofeng Wang, Xiaorui Zhou, Qian Zhang, Bingchao Xu, Jianru Xue, **2020**, "Image alignment based perceptual image hash for content authentication", international journal of Signal Processing: Image Communication, 80, 115642. Journal homepage: www.elsevier.com/locate/image

Su J., Vargas DV., and Sakurai K., **2018**, "One-pixel attack for fooling deep neural networks". arXiv. Available online at: https://arxiv.org/pdf/1710.08864.pdf. Accessed 24 Jan 2018.

Yuchun Fang, Yifan Li, Xiaokang Tu, Taifeng Tan, Xin Wang, **2020**, "Face completion with Hybrid Dilated Convolution", international journal Signal Processing: Image Communication 80,115664

L. Matteo, G. Mauger, A. Dazin, N. Tauveron, **2019**, "Modelling of a radial pump fast startup with the cathare-3 code and analyse of the loop response", in: Proceedings of 13th European Conference on Turbomachinery.

Russakovsky O., Deng J., Su H et al., **2015**, "Image Net Large Scale Visual Recognition Challenge". *Int J Comput Vis*, 115, pp. 211–252. CrossRefGoogle Scholar

Yosinski J., Clune J., Bengio Y., and Lipson H., **2014**, "How transferable are features in deep neural networks?", arXiv. Available online at: https://arxiv.org/pdf/1411.1792.pdf Accessed 25 Jan 2018.

D. Wilcox, **1986**. Multiscale model for turbulent flows, in: AIAA 24th Aerospace Sciences Meeting, American Institute of Aeronautics and Astronautics.

S. Melzer, S. Schepeler, T. Kalkkuhl, J. Friedrich, R. Skoda, **2019**, "Experimental investigation of transient characteristics of single-blade and two-blade pumps", in: Proceedings of 13th European Conference on Turbomachinery.

A. Weissenbrunner, A. Fiebach, S. Schmelter, M. Bnr, P.U. Thamsen, T. Lederer, **2016**, "Simulation-based determination of systematic errors of flow meters due to uncertain inflow conditions", international journal Flow Measurement and Instrumentation 52, 25–39. www.elsevier.com/locate/flowmeasinst

J. Steinbock, A. Weissenbrunner, M. Juling, T. Lederer, P.U. Thamsen, **2016**, "Uncertainty evaluation for velocity–area methods", international of Flow Measurement and Instrumentation 48, 51–56, www.elsevier.com/locate/flowmeasinst

V. T. Tran, H. T. Pham, B. S. Yang, and T. T. Nguyen, "Machine performance degradation assessment and remaining useful life prediction using proportional hazard model and support vector machine." Mechanical Syst. Signal Process., 32, 320 (**2012**).

C. Zhang and Y. Ma, in Ensemble Machine Learning (Springer, United States) (**2012**).

JürgenSchmidhuber, "Deep learning in neural networks: An overview.", Neural Networks, Volume 61, January 2015, Pages 85-117

SongchuanZhang, YoushenXia,WeixingZheng, "A complex-valued neural dynamical optimization approach and its stability analysis", Neural Networks,. Volume 61, January **2015**, Pages 59-67.

Oludare Isaac Abiodun, Aman Jantan, Oludare E Omolara, Muhammad Ubale Kiru, "Comprehensive Review of Artificial Neural Network Applications to Pattern Recognition", October **2019**, IEEE Access PP(99):1-1, DOI: 10.1109/ACCESS.2019.2945545.